Carbide and Nitride Overlayers on Early Transition Metal Surfaces: Preparation, Characterization, and Reactivities

Jingguang G. Chen

Corporate Research Laboratories, Exxon Research and Engineering Company, Annandale, New Jersey 08801

Received August 30, 1995 (Revised Manuscript Received December 5, 1995)

Contents

Jingguang G. Chen received his B.S. in Chemistry from Nanjing University, P.R. China, in 1982. He obtained his Ph.D. from the Surface Science Center, University of Pittsburgh, in 1988. During his graduate studies he was awarded the Mellon Predoctoral Fellowship by the University of Pittsburgh and the Varian Fellowship by the American Vacuum Society. He then spent one year as a Humboldt Postdoctoral Fellow in KFA-Jülich, Germany. He joined the Exxon Research and Engineering Company in 1989. He is currently a Staff Chemist in the Exxon Corporate Research Laboratories in New Jersey. He is also the Spokesperson for the Exxon U1A Beamline of National Synchrotron Light Source in Brookhaven National Laboratory. One of his primary research interests is to correlate the electronic and catalytic properties of transition metal carbides and nitrides and to apply these materials to industrial catalysis.

I. Introduction

Interstitial carbides and nitrides of early transition metals (groups IVB−VIB) are produced by dissolving carbon and nitrogen atoms into the metal lattices. These carbide and nitride materials have unique physical and chemical properties, which combine the characteristic properties of three different classes of materials: covalent solids, ionic crystals, and transition metals.[1−4] They demonstrate the extreme hardness and brittleness of covalent solids; they possess the high melting temperature and simple crystal structures typical of ionic crystals; and they have electronic and magnetic properties similar to transition metals. For example, carbides and nitrides are characterized by melting temperatures $\geq$3300 K and by values of hardness $\geq$2000 kg mm^{-2} and tensile strength $\geq$300 GPa, which are in the range of ceramic materials.[1] At the same time, values of their electric conductivity, magnetic susceptibility and heat capacity are in the metallic range.[1] The refractory and the conducting nature of carbides and nitrides makes them good candidates for various applications in material science.

Another application of carbides and nitrides of early transition metals is in heterogeneous catalysis. These materials often demonstrate catalytic advantages over their parent metals in activity, selectivity, and resistance to poisoning.[2−4] The catalytic properties of carbides and nitrides have been the subject of many experimental and theoretical investigations. Most of these studies were inspired by the pioneering work of Levy and Boudart,[5] who suggested that tungsten carbides displayed Pt-like behavior in several catalytic reactions. Subsequent investigations demonstrated that carbides and nitrides were good catalysts for a wide variety of reactions that typically utilized group VIII noble metals as catalysts. These studies indicated that for several types of reactions, such as hydrogenation reactions, catalytic activities of carbides and nitrides were approaching or surpassing those of noble metals.[3] Additional advantages for the catalytic applications of carbides and nitrides are related again to their refractory nature, which make them resistant to attrition and sintering under reaction conditions.

The existing and potential applications of early transition metal carbides and nitrides to both material science and catalysis have inspired many surface science investigations. The majority of these studies involves the preparation of thin carbide or nitride

S0009-2665(95)00232-9 CCC: $25.00

layers on the single-crystal surfaces of groups IVB−VIB transition metals. Comparing to bulk carbide/nitride single crystals, the advantages for choosing carbide/nitride overlayers as model systems are primarily 2-fold: (1) It allows one to directly compare the electronic properties and reactivities of the carbide/nitride overlayers with those of the parent metal surfaces, providing direct information on how the surface properties are modified as a result of carbide/nitride formation. (2) It enables one to readily control the nonmetal/metal stoichiometries and in some cases the structures of the carbide/nitride overlayers, while the crystalline orientations of bulk carbide/nitride single crystals are generally limited, due to experimental difficulties in cleaning procedures, to fcc(100), fcc(110) for carbides, and fcc-(100) for nitrides.[6]

In this review we will discuss primarily the preparation, characterization, and reactivities of carbide and nitride overlayers on the single crystal surfaces of groups IVB−VIB transition metals. The remainder of this review is organized as follows: In section II we will summarize the important properties of bulk carbides and nitrides by discussing the structural, electronic, and catalytic properties of these materials. The preparation procedures and thermal stabilities of carbide and nitride overlayers on single crystal surfaces will be reviewed in section III. In section IV we will discuss the characterization of the electronic properties of these overlayers. The reactivities of carbide and nitride overlayers will be summarized in section V by discussing the surface reactivities with several different classes of organic molecules. Finally, some potential research opportunities for surface science studies of transition metal carbides and nitrides, especially on the applications of these materials in catalysis and material science, will be briefly discussed in section VI.

We would like to point out that the preparation, characterization, and reactivities of carbide and nitride overlayers on single-crystal surfaces have been the subject of numerous experimental efforts and theoretical calculations. Due to the broad nature of this subject, it is inevitable that only a fraction of literature will be reviewed in this article. We do not intend to provide a chronological account of all research activities in this area. Rather, we will choose important examples to demonstrate the general similarities and differences of the surface properties of carbide and nitride overlayers.

II. Bulk Properties of Carbides and Nitrides

The properties of bulk carbides and nitrides have been discussed extensively in several recent review articles.[2−4,6−8] In this section we will briefly summarize the general observations related to the structural, electronic, and catalytic properties of bulk carbides and nitrides. The purpose of this brief summary is to provide the necessary background information, as well as motivations, for the surface science investigations of the chemical reactivities of carbide and nitride overlayers.

1. Structural Properties

Interstitial carbides and nitrides of early transition metals are often characterized by simple crystal structures. The metal atoms form lattices of face-centered cubic (fcc), hexagonal closed packed (hcp), or simple hexagonal (hex) structures, while carbon or nitrogen atoms reside in the interstitial sites between metal atoms.[1−4] These typical structures are shown in Figure 1. In general, carbon and nitrogen atoms occupy the largest interstitial sites available, i.e., the octahedral sites in fcc and hcp and the trigonal prismatic sites in hex structures.

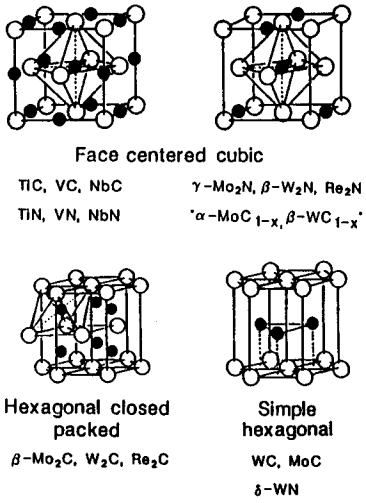

Figure 1. Typical structures of transition metal carbides and nitrides. The open and filled circles represent metal and nonmetal atoms, respectively. (Reprinted from ref 3. Copyright 1992 Elsevier.)

As summarized by Oyama,[3] the structures of carbides and nitrides are determined by two intimately connected factors, geometric and electronic. The geometric factor is based on the empirical rule by Hägg, which states that interstitial compounds will adopt simple structures (i.e., fcc, hcp, hex, etc.) when the ratio of hard-ball radii of nonmetal to metal is less than 0.59,[9] which is readily achieved in carbides and nitrides of groups IVB−VIB metals. Although these carbides/nitrides adopt simple crystal structures, they are typically different from those of the parent metals. For example, the structure of metallic molybdenum is bcc, but its stable carbide (Mo_2C) is hcp and its stable nitride (Mo_2N) is fcc. These structural differences between the parent metal and its carbide/nitride are explained by the electronic factor.[3] According to the Engel−Brewer theory, the structure of a metal or a substitutional alloy depends on the s−p electron count.[10,11] Qualitatively, as the s−p electron count increases, the structure transforms from bcc to hcp to fcc. In the case of carbides and nitrides, the mixing/rehybridization of the nonmetal s−p orbitals and the metal s−p−d orbitals would increase the total s−p electron count in the compound. The resulting s−p electron count would follow the order of parent metal < carbide < nitride, resulting in the structural transformations of Mo (bcc), Mo_2C (hcp), and Mo_2N (fcc). Similar trends are typically observed for other carbides and nitrides of groups IVB−VIB metals.

Recent structural investigations of single crystalline carbides and nitrides indicate that the surface and bulk structures of these materials are often different.[6] For example, the contraction of the first interlayer spacing was found to occur on the (111)

surface of several carbides. In addition, rippled relaxations and faceting were also observed on several carbide and nitride surfaces. More detailed information concerning the structural information of bulk carbides and nitrides can be found in a recent review article.[6]

2. Electronic Properties

Theoretical band calculations[12−14] of transition metal carbides and nitrides have indicated that the bonding in these compounds involves simultaneous contributions from metallic, covalent, and ionic bonding: the metallic bonding contribution is related to the rearrangement of metal−metal bonds; the covalent contribution is due to the formation of covalent bonds between metal and nonmetal atoms; and the ionic contribution is characterized by the charge transfer between metal and nonmetal atoms. In general, the two most important electronic properties are related to (1) the direction and amount of charge transfer and (2) the modification effect on the metal d-band upon the carbide/nitride formation.

The direction and amount of charge transfer in transition metal carbides and nitrides have been long-standing and sometimes controversial issues. Band−structure calculations, using the augmented plane wave (APW) method, indicate that the metal−nonmetal bonding contains a substantial amount of ionic character, which involves a charge transfer from metal to nonmetal.[15] Experimental results are often inconsistent. As pointed out by Ramqvist,[16] most of these experiments were carried out by studying the core level chemical shift using X-ray photoemission spectroscopy (XPS).[6,16−18] However, the correlation between the XPS chemical shift and the amount of charge transfer is complicated by the so called "nonchemical bonding" effects.[19] For example, in addition to the charge transfer in chemical bonding, the initial state effects also include change of the coordination of the substrate atoms. The latter effects usually lower the surface potential, which in turn alter the chemical shift in the XPS measurements.[19] In principle, this complication can be avoided to a certain degree by using the near-edge X-ray absorption fine structure (NEXAFS) technique, as recently demonstrated for the investigation of charge transfer in vanadium carbide.[20] At present, the general agreement concerning the direction of charge transfer in carbides and nitrides is from metal to nonmetal atoms. The ionicity of the carbides/nitrides, which is determined by the amount of charge transfer, increases as the parent metals move from groups VIB to IVB. This trend is believed to be related to the decrease in the electronegativity of the parent metals.[3,16]

The formation of carbides and nitrides modifies the nature of the d band of the parent metal, which in turn gives rise to catalytic properties that are different from those of the parent metals but similar to those of group VIII noble metals.[3] One simple explanation is related to the fact that, upon the formation of interstitial compounds, the metal lattice expands and the metal−metal distance increases. For example, after carbide formation, the lattice constants of vanadium are expanded from 0.26 to 0.42 nm and for molybdenum from 0.27 to 0.30 nm, respectively. The increase in the metal−metal bond distance would result in a contraction of the metal d band,[21] which was estimated by Heine to be proportional to the inverse fifth power of the metal−metal distance.[22] It is believed that such a d-band contraction would result in a greater density of states (DOS) near the Fermi level, as compared to the parent metal, despite the charge transfer from the metal to the carbon/nitrogen atoms. As will be discussed later, more recent band structure measurements[6] and calculations[23] indicated that the formation of metal−carbon and metal−nitrogen bonds resulted in significant redistributions of the density of states (DOS) both below and above the Fermi level. These results also demonstrated that the redistributions of the DOS in carbides/nitrides could vary significantly for differently oriented planes and for different adsorbates.[6,23]

Among early transition metal carbides and nitrides, the electronic properties of WC have been extensively investigated by various experimental techniques.[24−26] As pointed out earlier, most of these studies were inspired by the pioneering work of Levy and Boudart,[5] who suggested that tungsten carbides displayed Pt-like behavior in several catalytic reactions. These studies[24−26] were carried out by comparing the electronic properties of W before and after carbide formation. Overall, these studies suggested that the modification of the W d-band might be very complicated, with the filled and unfilled states of the d band being modified by a different manner as a result of carbide formation. For example, by using XPS,[24,25] the filled states of the W d band were found to be narrowed after carbide formation, resulting in similar electronic structures of WC and Pt up to the Fermi level. On the other hand, at energies above the Fermi level, the width of the unfilled states of the d-band of W was found to be broadened due the formation of WC,[26] giving rise to a greater density of empty levels for WC than those of parent W. More about the electronic modifications on the filled and unfilled states of the d band, and their effects on the surface reactivities, will be discussed later.

More detailed investigations concerning the band structures of both filled and unfilled DOS of the d band have been carried out extensively for bulk single-crystal carbides and nitrides, by using angle-resolved photoemission (ARP) and inverse photoemission (IPE) techniques, respectively,[6] These studies revealed the presence of a variety of density of states both below and above the Fermi level; details concerning the various bulk and surface electronic states of single crystalline groups IVB−VIB transition metal carbides and nitrides have been discussed in a recent review article.[6] However, these detailed band structure investigations have not been applied to directly compare the electronic properties of a metal surface before and after the carbide/nitride formation. At present, the lack of direct comparison between the parent metal and its carbide/nitride prevents one from concluding how the band structures of the parent metals are modified as a result of carbide/nitride formation.

3. Catalytic Properties

Early transition metal carbides and nitrides have been demonstrated to have excellent catalytic activities in a variety of reactions,[2,3] including hydrogenolysis, hydrogenation, dehydrogenation, isomerization, methanation, hydrodesulfurization (HDS), hydrodenitrogenation (HDN), and ammonia synthesis. One of the primary interests in the applications of carbides and nitrides in these reactions was to use them as cheaper alternative catalysts to replace group VIII noble metals. In many instances the catalytic activities of carbides/nitrides resemble those of noble metals. For example, for hydrogenation[3,27] and hydrogenolysis[3,28,29] types of reactions, carbides/nitrides demonstrate catalytic activities that are similar to or larger than those of noble metals. Experimental results also indicated that carbides and nitrides might even be more desirable catalysts than these metals for certain types of reactions. For example, carbides/nitrides often showed unique catalytic pathways, producing desirable product selectivities.[3,29] Another potential catalytic advantage of carbides/nitrides is that they often show higher sulfur[3,30,31] and nitrogen tolerance than the noble metals.[3,32]

Both theoretical[23] and experimental investigations[33−35] indicated that the reactivities of bulk carbides could differ drastically for differently oriented surfaces. For example, different reactivities were observed for NbC(100) and NbC(111),[33] and for TiC(100)[34] and TiC(111).[35] Figure 2 shows a comparison of the unreconstructed (100) and (111) surfaces of bulk TiC, which is characterized by the NaCl structure with two interpenetrating Ti and C fcc lattices.[23] While the (100) surface is characterized by the coexistence of both Ti and C, the (111) orientation gives rise to alternative layers of Ti and C. By using O_2, CO, and CH_3OH as probing molecules,[33−35] the general observation was that the reactivity of the TiC(111) surface was very similar to that of titanium metal, while the reactivity of the TiC(100) surface was significantly reduced and was similar to those of Pt group metals. This aspect will be discussed in more detail in conjunction with the band structure calculations of TiC(100) and TiC(111).

The reactivity of the bulk carbide materials was also found to be related to the nature of surface carbon species.[36−39] For example, the presence of so-called "free carbon", which was characterized by surface spectroscopies to be amorphous or graphitic in nature,[39] reduced the catalytic reactivity. This was demonstrated clearly in earlier electrochemical investigations of the reactivity of carbide electrodes.[37−41]

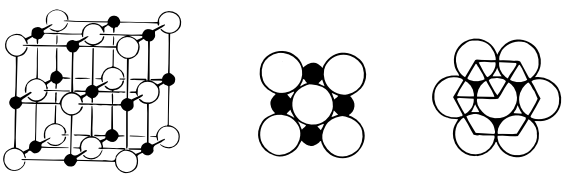

Figure 2. A comparison of the structures of the (100) and (111) orientations of TiC. The large open circles and small filled circles represent Ti and C atoms, respectively. (Reprinted from ref 23. Copyright 1988 Elsevier.)

By controlling the preparation methods, the electrocatalytic reactivity of the carbide electrodes was found to be directly related to the amount of "free carbon".[37−39] Recent studies also indicated that the catalytic reactivity of carbides could be enhanced by removing the excess amount of "free carbon" with oxygen.[42]

For the catalytic reactivities described above, fundamental understanding concerning the reaction mechanisms over carbides/nitrides is not as well established as for metal surfaces. The application of powerful surface science spectroscopies on well-characterized carbide/nitride overlayers should provide important insights into the fundamental understanding of the surface reactivities of this important class of catalytic materials. The remainder of this article will concentrate on how to prepare and characterize these model carbide/nitride systems and will attempt to correlate the surface reactivities to the underlying electronic properties of the carbide/nitride catalysts.

III. Preparation of Carbide and Nitride Overlayers

1. Carbide-Modified Surfaces

Carbide-modified surfaces have been produced on single-crystal faces of several early transition metals. Table 1 summarizes a selected list of carbide-modified surfaces of V(110),[20,43−46] Ta(110),[47] Mo(100),[48−56] Mo(110),[57−60] Mo(111),[61] W(100),[62−76] W(110)[62,77−80] and W(111).[62,81] Also compared in Table 1 are the observed LEED patterns and the corresponding carbon/metal surface atomic ratios. The most common practice for the production of carbide-modified surfaces is the thermal cracking of hydrocarbon molecules such as ethylene. The most efficient temperature for the thermal cracking varies from metal to metal, although annealing to temperatures above 600 K is often required to obtain sharp LEED patterns. In general, there are three important aspects related to the characterization of carbide overlayers: the surface structure, the local bonding environment of carbon atoms, and the thermal stability of the carbide overlayer. In the following we will use specific examples to demonstrate how these issues can be addressed experimentally.

Since the crystal structures of bulk carbides are generally different from those of the parent metals,

Table 1. Preparation and Characterization of Carbide-Modified Surfaces of Early Transition Metals

surfaces	ref(s)	LEED patterns	carbon/metal surface ratios
V(110)	20, 43−46	none	1.0
Ta(110)	47	none	2.0
Mo(100)	48−56	c(2×2)	0.5
		c(3√2×√2)R45°	0.67
		p(1×1)	1.0
Mo(110)	57−60	p(4×4)	0.37
Mo(111)	61	p(6×1)	
W(100)	62−76	c(2×2)	0.5
		c(3√2×√2)R45°	0.67
		p(6×1)	
		p(5×1)	0.8−1.2
W(110)	62,77−80	p(15×3)R14°	0.64
W(111)	62	none	

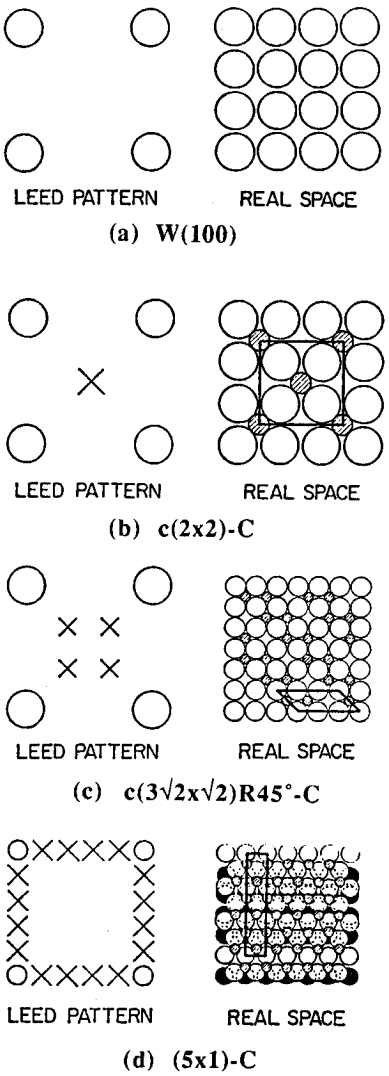

Figure 3. The LEED patterns and real space interpretations of (a) W(100), (b) c(2×2)-C, (c) c(3√2×√2)R45°-C, (d) p(5×1)-C overlayers. The open and shaded circles represent W and carbon atoms, respectively; the dark circles for the (5×1)-C overlayer represent W atoms in the second layer. (Reprinted from ref 64. Copyright 1978 Academic.)

carbide overlayers are often characterized by complicated LEED patterns, especially at high carbon coverages. The overlayer structures and corresponding surface carbon/metal ratios can be determined by using the combination of LEED, Auger electron spectroscopy (AES), and other surface sensitive spectroscopies such as alkali-ion scattering.[75] Figure 3 shows the LEED patterns and real space interpretations of several carbide overlayer structures on W(100). For example, a c(2×2)-C/W(110) layer was produced by exposing to ethylene at room temperature followed by annealing to 1000 K. The C/W surface atomic ratio of this overlayer was determined from the LEED and AES analysis to be 0.50. Further exposure to ethylene at room temperature splitted the c(2×2) spots into four lobes moving outward along the diagonals of the (1×1) pattern, eventually resulting in a pattern that could be described as c(3√2×√2)-R45°.[64,75] The C/W surface ratio of this layer was estimated to be 0.67. Heating the W(100) surface to 1500 K in ethylene eventually led to the formation of a p(5×1) LEED pattern. The p(5×1) pattern was interpreted as a reconstructed structure, with a

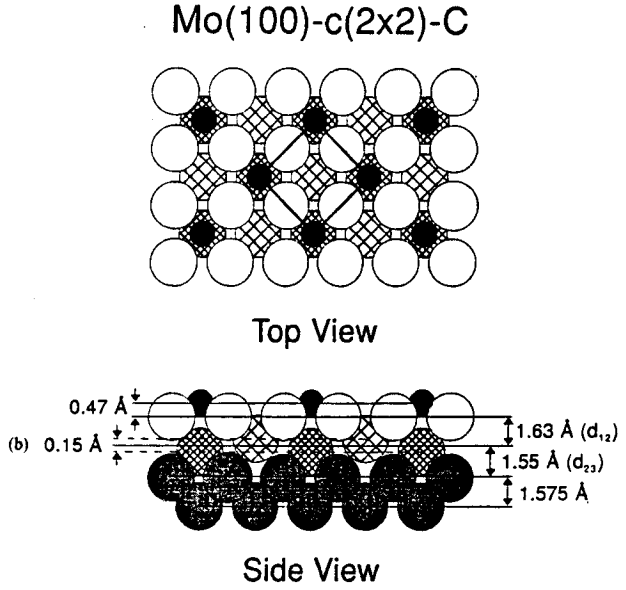

Figure 4. Surface structures of a c(2×2)-C/Mo(100) overlayer determined from a Tensor LEED measurement. (Reprinted from ref 56. Copyright 1995 Elsevier.)

(0001) W_2C overlayer coincident on the tungsten (100) substrate.[62−64] The carbon atoms were believed to occupy the interstitial sites between the first two reconstructed tungsten layers to produce the W_2C local stoichiometry. The C/W surface atomic ratio of the p(5×1) surface was estimated, from a combined LEED and AES analysis, to be ∼0.76−0.80 for an unreconstructed C/W(100) surface and to be 1.2 if the carbide overlayer was reconstructed.[64] Similar C/W ratios were obtained by using the surface-sensitive angle-resolved alkali ion scattering technique,[75] which estimated that the C/W ratios were 0.45 ± 0.05, 0.63 ± 0.06, and 0.80 ± 0.06 for the c(2×2), c(3√2×√2)-R45°, and p(5×1) overlayers, respectively. The major discrepancy, however, was that the alkali ion scattering data suggested that carbon atoms were situated on or near the 4-fold hollow sites at all carbon coverages and the W(100) substrate did not undergo any reconstruction even for the p(5×1) overlayer.[75] The observation of the p(5×1) LEED pattern was attributed by these authors to an ordering in the carbon overlayer and a possible small amplitude periodic strain in the first layer of W as a result of carbide formation.[75] More precise structural tools, such as the Tensor LEED method as will be discussed below,[56] should provide a definitive answer on whether and/or how the p(5×1)-C/W(100) surface is reconstructed.

Much more detailed information concerning the overlayer structures of carbides can be obtained by comparing dynamical calculations with intensity−voltage (I−V) LEED measurements.[56] Jentz et al. have recently applied an automated Tensor LEED (TLEED) method to determine the local structure of a c(2×2)-C overlayer on a Mo(100) surface.[56] As shown in Figure 4, the TLEED measurements reveal that carbon atoms occupy the 4-fold hollow sites of Mo(100) at 0.47 Å above the Mo plane. In addition, Figure 4 provides important information on the structures of the Mo(100) substrate. For example, it shows a relatively large buckling of 0.15 ± 0.06 Å for Mo atoms in the second layer, with the Mo atom

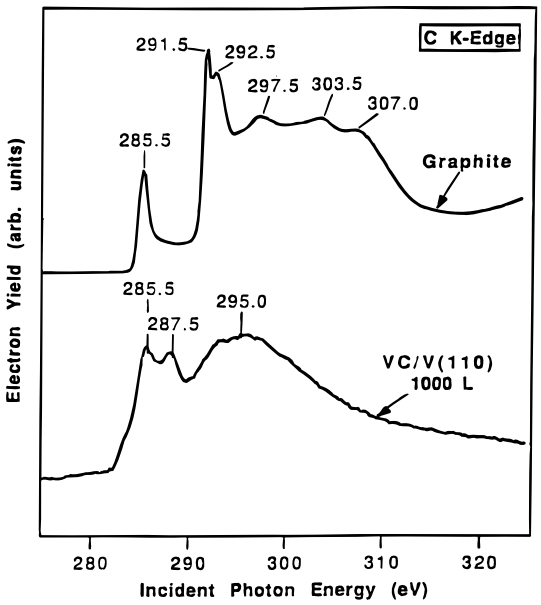

Figure 5. Comparison of K-edge features of carbide-modified V(110) and graphite. The carbide overlayer was prepared by exposing V(110) at 600 K to 1000 L of ethylene. (Reprinted from ref 20. Copyright 1994 Elsevier.)

beneath the C being displaced downward and the Mo atom beneath the unoccupied hollow site being moved upward. Figure 4 also shows that the average interspacing between the first and second layers of the c(2×2)-C surface is 1.63 ± 0.06 Å, which is expanded relative to the first interspacing of clean Mo(100) of 1.49 Å.[56] Similar dynamical LEED measurements for other carbide overlayers, especially for those with complicated LEED patterns, will substantially enhance our understanding of the structural aspects of these surfaces.

The local bonding environment of carbon atoms in carbides, as compared to that in other forms of carbon species such as graphite, diamond, or carbonaceous materials, can be distinguished by several techniques. The definition of carbidic carbon here is that it is bonded to metal atoms instead of to other carbon atoms. The carbidic nature can be generally identified either by the characteristic C(KLL) transitions in AES measurements[82,83] or by the characteristic chemical shift in XPS measurements.[16,60] An alternative, and probably more sensitive, method for characterizing the carbidic nature of carbon species is the utilization of NEXAFS. Figure 5 shows a comparison of the carbon K-edge features of a VC/V(110) overlayer and graphite.[20] The VC/V(110) surface is characterized by two sharp near-edge features at 285.5 and 287.5 eV and a broad feature at ~295 eV, respectively. It is clear that the number of K-edge features, as well as their energy positions, of the VC/V(110) surface are drastically different from those of graphite. Since the carbon K-edge features are related to the electronic transitions of C 1s electrons to a set of partially filled and unfilled orbitals, the number of peaks and their positions are highly specific to the local bonding configurations of carbon atoms.[84] Therefore, the carbon K-edge features of various carbon-based compounds, such as graphite,[84,85] diamond,[84,86] and plasma-generated[87] or argon-sputtered carbonaceous carbon films[88] are qualitatively different from those of VC/V(110).

The NEXAFS technique also has other advantages for the characterization of carbide overlayers. One of them is that it can readily measure materials in the forms of either single-crystal surface or powder materials. This allows one to compare the model carbide or nitride surfaces directly to standard powder compounds, as has been done for vanadium carbides.[89] By comparing the NEXAFS data of VC/V(110) in Figure 5 to the existing band−structure calculations,[90,91] the C K-edge features can be assigned to the excitation of C 1s electrons to the partially filled and unfilled orbitals that are resulting from the hybridization of C 2p orbitals and V 3d orbitals.[89−91] The two sharp resonances at 285.5 and 287.5 eV can be assigned to the transitions of C 1s electrons to the p−d(t_{2g}) and p−d(e_g) hybridized orbitals of vanadium carbide, respectively. Similarly, the broad feature at ~295 eV can be assigned to the excitation of C 1s electrons to an unoccupied orbital that involves contributions from 2p and 3p orbitals of carbon and the d and s states of metals.[90,91]

Another advantage of using NEXAFS is that it can differentiate the surface and bulk compositions of carbide materials, which can be achieved by comparing the NEXAFS spectra recorded by means of the electron−yield and fluorescence−yield methods.[20,92] Although both measurements provide information on the local environment of carbon, the probing depths of the two methods are very different. Similar to the AES or XPS measurements, the mean free path in the electron−yield measurement is roughly 10 Å.[93] On the other hand, the detection limit of the fluorescence−yield method is significantly deeper, because the mean-free path of the C K_α X-ray photons is approximately 1500 Å.[94] Such a comparative investigation is particularly important when the average thickness of carbide overlayer is greater than the mean free path of the C(KLL) Auger electrons or the C 1s XPS photoelectrons.[60] For example, Figure 6 shows a comparison of electron−yield and fluorescence−yield NEXAFS spectra of several C/Mo(110) overlayers with different carbon coverages.[60] The bottom spectra were obtained after the Mo(110) surface was exposed to 10 L of ethylene at 100 K and subsequently heated to 1200 K. Such a treatment resulted in a well-ordered p(4×4) LEED pattern.[59] The middle spectra were obtained from a surface exposed to 300 L of ethylene at 600 K and heated to 1200 K ("1-cycle carbide"). The top spectra were acquired after five such dosing/annealing cycles ("5-cycle carbide"). The C K-edge features of C/Mo(110) are characterized by two sharp resonances at 285.5 and 288.0 eV. Similar to the assignment of VC, these two NEXAFS features can be assigned to the transitions of C 1s electrons to the p−d(t_{2g}) and p−d(e_g) hybridized orbitals of molybdenum carbide, respectively.[89] In NEXAFS measurements, the elemental concentration can be derived from the height of the edge-jump;[84] the relative concentrations of the C/V(110) overlayers in Figure 6 can be compared by the heights of the edge-jump from 275 to 315 eV. Although the NEXAFS spectra show an increase in the edge-jump with increasing dosing/annealing cycles in both the electron−yield and fluorescence−yield measurements, the magnitude of the increase

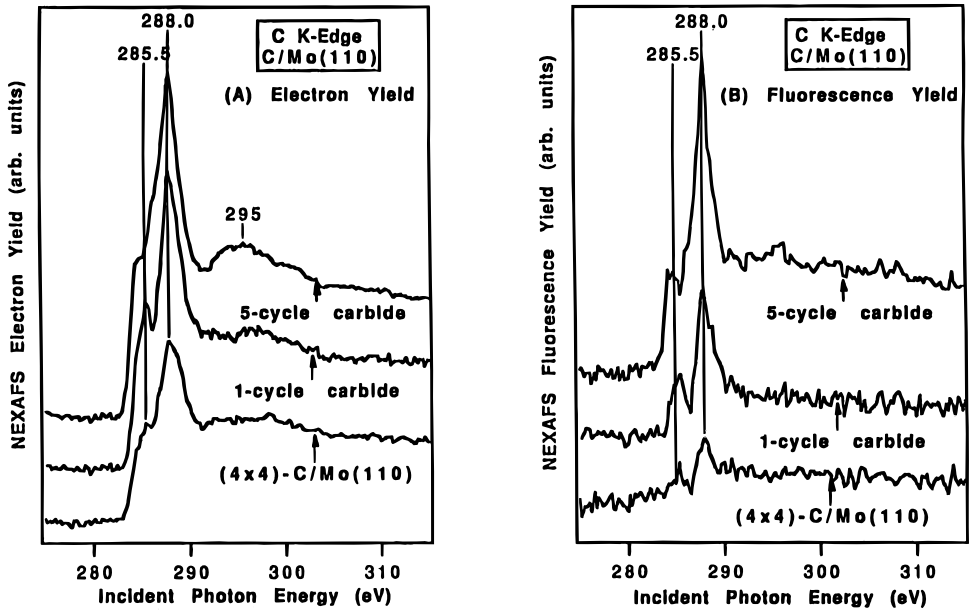

Figure 6. A comparison of NEXAFS data of C/Mo(110) overlayers by measuring the surface-sensitive electron yield and the bulk-sensitive fluorescence yield. (Reprinted from ref 60. Copyright.)

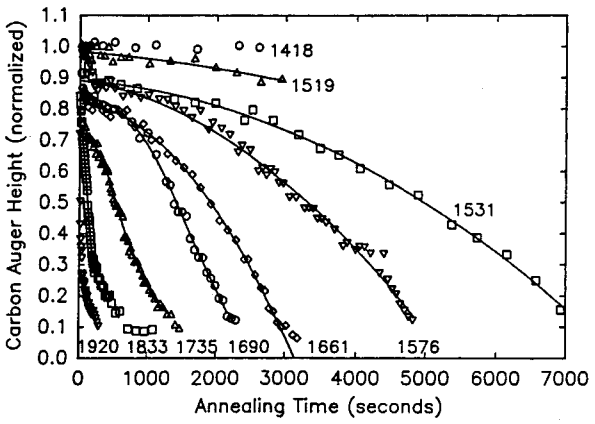

Figure 7. Normalized AES C(KLL) intensity of C/W(110) as a function of annealing time at various temperatures. (Reprinted from ref 79. Copyright 1990 Elsevier.)

is much larger in the bulk-sensitive fluorescence−yield measurement. Such a comparison clearly indicates that carbide overlayers, with an average thickness greater than 10 Å, are produced after repeated cycles of exposing Mo(110) to ethylene at 600 K followed by annealing to 1200 K.[60]

Upon heating a carbide overlayer, a fraction of the carbon atoms undergoes a thermally induced diffusion into either the subsurface sites or the metal bulk. The inward diffusion of carbon atoms has been observed for several early transition metals such as Ti,[95] Zr,[96] V,[20,46] Mo,[49,59−61] and W.[64,79] These conclusions were based primarily on the observation of a decrease in the intensities of either the C(KLL) Auger transition or the C 1s XPS peak. At sufficiently high temperatures, carbide overlayers decompose and all carbon atoms subsequently diffuse into the metal bulk. The kinetics for carbide decomposition and subsequent carbon diffusion on W(110) have been investigated in detail by Sunderland and Slavin. Figure 7 shows peak intensities of the C(KLL) Auger feature recorded as a function of annealing time at various temperatures.[69] At temperatures above 1531 K, a typical time-resolved curve indicated that the C(KLL) intensity underwent a rapid decrease to a plateau value of 0.85, which was attributed to the reorganization of the carbide overlayer.[79] Further decrease in the C(KLL) intensity was due to the diffusion of carbon into the bulk. As demonstrated from these time-resolved measurements, the diffusion rate gradually increased at first, which was followed by a decrease at low carbon concentrations. Such kinetic behavior could be readily modeled by describing the carbide overlayer as a monolayer containing holes and by considering that the decomposition of carbide occurred only at the peripheries of these holes. At a fixed temperature, the decomposition rate should be proportional to the hole perimeter. Therefore, the carbide decomposition rate should gradually increase until the holes coalesce; the resulting islands should then decrease in perimeter, giving rise to a decrease in the decomposition rate until all carbon atoms disappear.[79] The thermal decomposition also occurs for other carbides, although the decomposition temperature depends strongly on the specific metal substrate. For example, on V(110), the decomposition of vanadium carbide and subsequent carbon diffusion start to occur at 925 K,[46] which is about 500 K lower than that observed on W(110).[79]

2. Nitride-Modified Surfaces

Nitride-modified surfaces have been produced on groups IVB−VIB early transition metals such as Ti,[97−104] Zr,[94,105] Hf,[105] V,[105] Nb,[105−109] Ta,[105, 109,110] Cr,[111−114] Mo,[115−119] and W.[120−127] Surface nitrogen atoms were produced by exposing the metal surfaces to either NH_3 or N_2, generally in the temperature range of 300 to 900 K. Molecular beams of NH_3 and N_2 have also been used to produce nitride-modified surfaces on W(110).[122,124,127] The decomposition rates of NH_3 and N_2 were found to be dependent on the surface orientations of both Mo and W. A detailed analysis of the reaction kinetics and thermodynamics of the decomposition of NH_3 or N_2 on Mo was given by Boudart et al.[127] On the low-index single-crystal

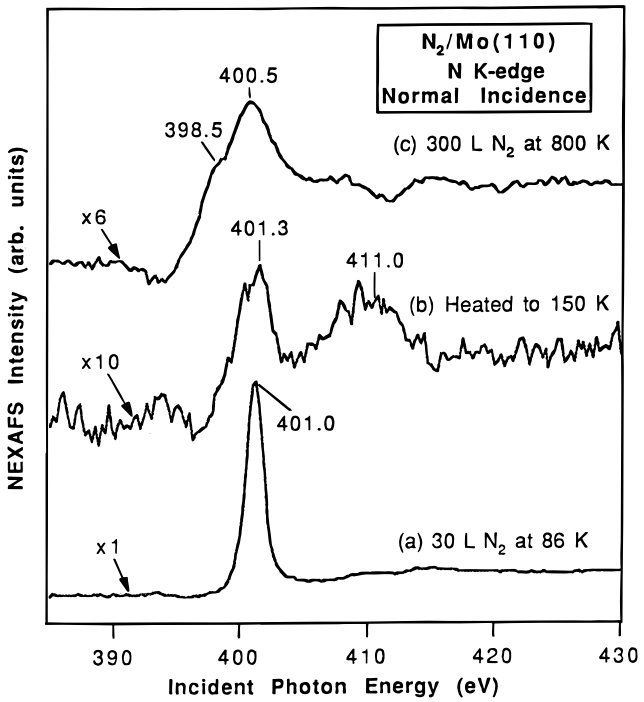

Figure 8. Comparison of N K-edge features of molecular and atomic nitrogen species on Mo(110). The NEXAFS data were recorded with the crystal surface normal to the photon beam (from ref 118).

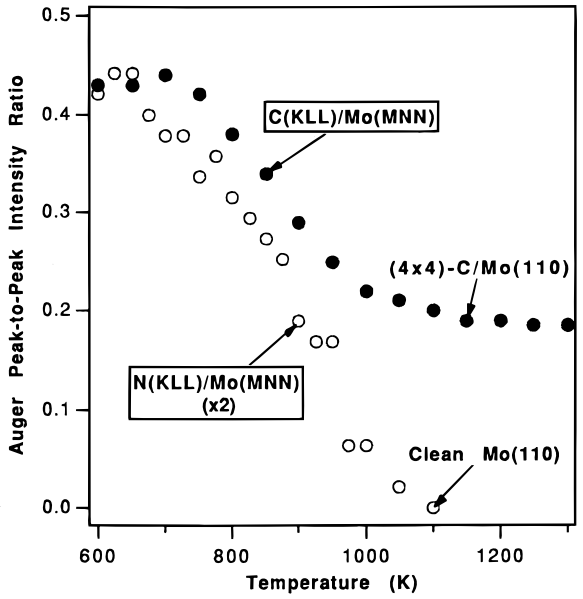

Figure 9. Different thermal behavior of carbide- and nitride-modified Mo(110) surfaces. For the purpose of comparison, the atomic ratios of C/Mo and N/Mo at 600 K are approximately estimated by using the AES sensitivity factors to be 0.84 and 0.22, respectively. (Reprinted from ref 60. Copyright.)

surfaces, several well-characterized overlayer structures have been reported, including p(1×1)-N/Ti-(0001),[101,102] p(5×5)-N/Nb(100),[106,108] p(1×1)-N/Cr-(100),[112] c(2×2)-N/Mo(100),[116] c(3×2)-N/Mo(111),[119] p(2×2)-N/W(110),[122,123] and p(4×2)-N/W(110).[127]

A novel way of depositing thin films of molybdenum nitride has been utilized by Thompson and coworkers.[128−130] A series of well-characterized Mo nitride films were evaporated onto a Si(100) single crystal using ion beam-assisted deposition (IBAD). By varying the experimental conditions, these authors were able to generate well-characterized nitride thin films with different N/Mo stoichiometries, such as β-$Mo_{16}N_7$, γ-Mo_2N, and δ-MoN.[130] Another important aspect of the IBAD method is its capability to generate nitride films with preferentially oriented crystalline planes, with respect to the Si(100) substrate. For example, the crystalline planes for β-$Mo_{16}N_7$, γ-Mo_2N, and δ-MoN films were preferentially oriented along the (400), (200), and (101) directions, respectively.[128−130]

The local bonding environment of nitrogen can be probed by using NEXAFS. The characteristic set of N K-edge features of nitride[89−91] can be readily differentiated from those of nitrogen atoms in N_2[131] or NH_3.[132] For example, Figure 8 shows a comparison of the N K-edge features, recorded at normal incidence, of N_2 molecules on Mo(110) to those of nitride.[118] The molecular N_2 species adsorb either perpendicular (Figure 8a) or parallel (Figure 8b) to the Mo(110) surface, depending on the experimental conditions. These two molecular species were identified by using the polarization-dependence NEXAFS and by vibrational spectroscopies.[118] The nitride-modified surface (Figure 8c) was prepared by exposing the Mo(110) surface to 300 L (1 L = 1×10^{-6} Torr s) of N_2 at 800 K. The nitride-modified surface is characterized by two relatively broad features at 398.5 and 400.5 eV, respectively, which are qualitatively different from the peak positions of molecular N_2 species. However, Figure 8c is very similar to the NEXAFS spectra of bulk nitrides of groups IVB−VIB metals.[89−91,133] Similar to that discussed for carbides, the two resonances in Figure 8c can be assigned to the transitions of N 1s electrons to the hybridized (N 2p + Mo 4d) orbitals of molybdenum nitride.[89,133]

The occupation of N atoms in the interstitial sites, resulting from the inward diffusion of nitrogen atoms, has also been proposed for Ti,[101,102] Zr,[94] Nb,[106−109] and W.[121−123] However, the thermal behavior of nitride overlayers on single-crystal surfaces is sometimes different from that of carbide overlayers. While carbon atoms diffuse into the subsurface sites and/or the metal bulk at higher temperatures, nitrogen atoms can either diffuse into the bulk or recombine to desorb as N_2 molecules. For example, Figure 9 shows a comparison of the thermal stability of carbide- and nitride-modified Mo(110) surfaces.[60] The two overlayers were prepared by exposing Mo(110) at 600 K to 100 L of C_2H_4 and NH_3, respectively. For ease of comparison, AES peak-to-peak intensity ratios of C(KLL)/Mo(MNN) and N(KLL)/Mo(MNN) are normalized to the same value at 600 K. Although the carbide overlayer initially undergoes a thermal diffusion in the temperature range of ~700−1000 K, the AES C/Mo intensity ratio reaches a constant value (0.19−0.21) in the temperature range of 1100−1300 K. The LEED investigation reveals that the carbide overlayers in this temperature range is characterized by a sharp (4×4)-C pattern,[59] indicating the presence of a well-characterized carbide overlayer after annealing. The thermal behavior of the nitride-modified surface, on the other hand, is very different. The AES intensity ratio of N/Mo starts to decrease at ≥700 K and eventually reaches zero at 1100 K, producing an atomically clean Mo-

(110) surface at this temperature. The corresponding temperature-programmed desorption (TPD) measurement reveals[118] that all nitrogen atoms recombine to desorb molecularly. One of the implications from Figure 9 is that nitrogen atoms are occupying only the surface sites on Mo(110); the thermally induced diffusion of nitrogen into the subsurface region is prevented due to the competition from the recombination and subsequent molecular desorption. The absence of subsurface/interstitial nitrogen suggests that the nitride-modified Mo(110) overlayer would not correctly model the reactivities of bulk molybdenum nitrides. This important aspect will be discussed later in the different surface reactivities of carbide and nitride overlayers on Mo(110).

IV. Characterization of Carbide and Nitride Overlayers

1. Ionic and Covalent Nature of Metal–Nonmetal Bonding

As mentioned earlier, the metal−nonmetal bonding in carbides and nitrides consists of both ionic and covalent contributions. It is proposed for bulk carbides and nitrides[2] that the degree of ionic contribution is related to the electronegativity difference between the metal and carbon or nitrogen, which increases from group IVB to group VIB. The ionic contribution in a chemical bond can be qualitatively judged by the degree of charge transfer between the two atoms that are producing the bond. The relationship between the electronegativity and charge transfer has been discussed by Sanderson,[134] who postulates that when two atoms bond together electron transfer occurs to adjust their electronegativities to a common intermediate value. This postulate was also supported by density functional theory calculations.[135] This relationship was also observed experimentally for adsorbed atoms on surfaces by Grant et al.[52] For example, by following the XPS core level shifts in the Mo(3d) transitions, these authors found a linear relationship between the electronegativity of the adsorbed atoms (B, C, and O) and the amount of charge transfer from Mo to these adatoms.

In principle, the direction and the amount of charge transfer in the metal−nonmetal bond can be estimated from the oxidation state of the metal. Figure 10 shows a comparison of NEXAFS investigations of the oxidation states of vanadium and molybdenum in carbide overlayers. These carbide overlayers were prepared by exposing the metal surfaces to over 600 L of ethylene at 600 K to generate relatively thick carbide layers;[20] the NEXAFS measurements were carried out at glancing incidence (75° from surface normal) to minimize contributions from the metal bulk. Figure 10a shows the peak position of the vanadium L_{III} NEXAFS feature, which is related to the electronic excitations from $2p_{3/2}$ to 3d orbitals.[20] By comparing the V L_{III} peak position of the carbide overlayer to those of clean V(110) and several standard compounds, including V_2O_3, V_2O_4, and V_2O_5, the oxidation state of vanadium in VC can be estimated to be $V^{1.2\pm0.2}$. This observation indicates that the direction of charge transfer is from vanadium to carbon and the amount of charge transfer is approximately 1.2 ± 0.2 electrons per vanadium, clearly indicating a significant amount of ionic contribution in the V−C bond.[136]

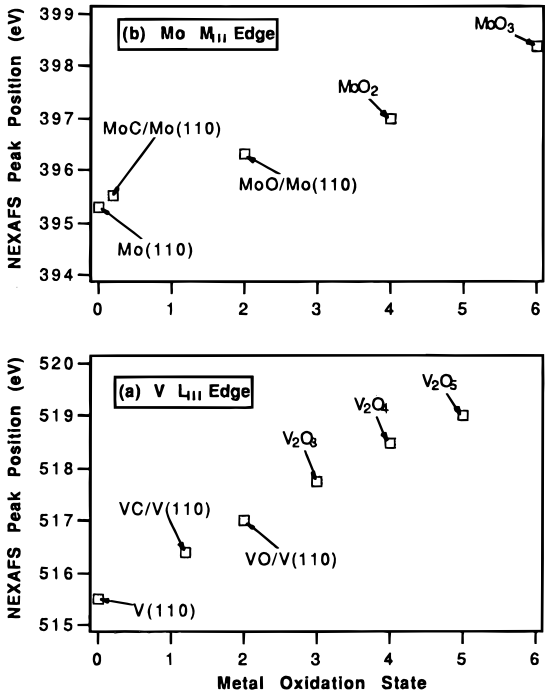

Figure 10. NEXAFS determination of the oxidation states of carbide overlayers on (a) V(110) and (b) Mo(110). The two carbide layers were prepared by exposing V(110) to 1000 L and Mo(110) to 600 L of ethylene at 600 K; the NEXAFS measurements of these overlayers were recorded at glancing incidence. (Reprinted from ref 20. Copyright 1994 Elsevier.)

Similar NEXAFS measurements were carried out for a carbide overlayer on Mo(110), as shown in Figure 10b. The peak position of the Mo M_{III} feature, which is related to an electronic transition from $3p_{3/2}$ to 4d orbitals, of Mo carbide is compared to those of clean Mo(110) and model compounds of MoO_2 and MoO_3.[136] Figure 10b shows that the M_{III} peak position of the carbide overlayer is very close to that of clean Mo(110); the oxidation state of Mo in the carbide overlayer is approximately $Mo^{0.2\pm0.2}$. This observation therefore suggests that the ionic contribution in the Mo−C bond is relatively small, supporting the argument that the ionic contribution is larger in groups VB carbides than in group VIB carbides.[2,16]

2. Band Structures of Carbide/Nitride Overlayers

One of the most important aspects related to the electronic properties of carbide/nitride is the modification of the parent metal d band by the formation of carbide/nitride overlayers. A direct comparison of the characteristics of the metal d band *before and after* carbide/nitride formation would significantly enhance our understanding of the electronic properties and their roles in determining the chemical reactivities of carbide/nitride materials. In general, band structure investigations are carried out by using angle-resolved photoemission (ARP) spectroscopy for the filled states and inverse photoemission (IPE) spectroscopy for the unfilled states. These two techniques have been extensively applied to the band

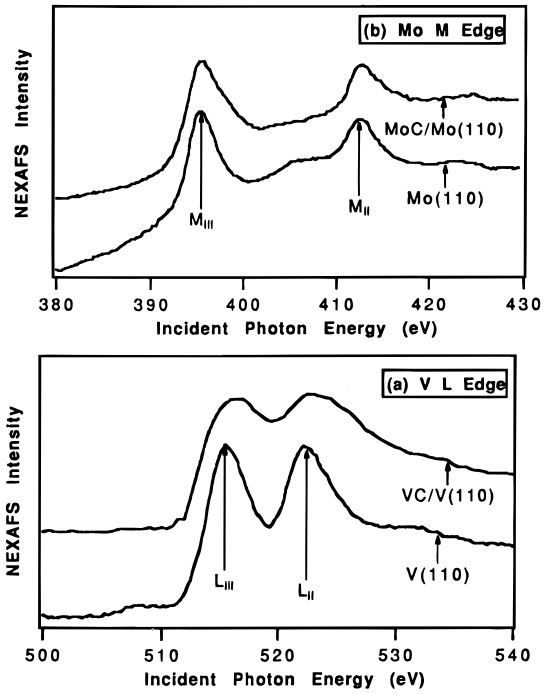

Figure 11. The V L-edge and Mo M-edge transitions of carbide overlayers on (a) V(110) and (b) Mo(110). (Reprinted from ref 20. Copyright 1994 Elsevier.)

structure investigations of the bulk carbides and nitrides.[6] However, systematic band structure measurements on carbide/nitride overlayers are lacking at present.

The d-band occupation near the Fermi level of clean W(100) and the p(5×1)-C/W(100) surfaces was compared by using photon energy-dependent valence-band photoemission spectroscopy.[76] The electronic structure of the tungsten surface was found to be altered by the formation of carbide, as indicated by a deficiency in the d-band occupation near the Fermi level for the p(5×1)-C/W(100) overlayer. Furthermore, the valence band spectrum of the p(5×1)-C/W(100) surface was determined to be essentially identical to WC(0001).[76] One of the consequences of the deficiency in the d-band occupation near the Fermi level is that the carbide surface would have a reduced ability to donate d electrons to adsorbates; this subject will be discussed in detail in the section 4.3.

Several other experiments also provided evidence that the valence band structures of early transition metals were very sensitive to the formation of metal−carbon and metal−nitrogen bonds. For example, Fukuda et al. found that a UPS peak at 1.4 eV below the Fermi level of Ti(0001) disappeared when the surface was exposed to N_2 or CO at room temperature,[93] most likely due to the formation of Ti−N and Ti−C/Ti−O bonds, respectively. In addition, by using soft X-ray appearance potential spectroscopy, Nyberg found that the DOS of the unfilled d band of Cr, Mo, and W were also modified due to the formation of metal−carbon and metal−nitrogen bonds.[137]

The NEXAFS technique was also utilized to characterize the DOS of the unfilled metal d band before and after the formation of carbide overlayers on V(110) and Mo(110).[43,136] Figure 11a shows a comparison of vanadium L-edge features of V(110) and C/V(110). The preparation conditions of VC/V(110) and the experimental conditions for NEXAFS measurements were the same as those described in Figure 10a. Since the L-edge features involve the electronic transitions from the $2p_{3/2}$ (L_{III}) and $2p_{1/2}$ (L_{II}) states to the unfilled states of the vanadium d band, one could argue that the peak widths of these transitions are primarily determined by the characteristics of the DOS of the unfilled d band. As shown in Figure 11a, the L_{III} and L_{II} near-edge features of V(110) are relatively intense and well-resolved for metallic vanadium at 515.5 and 522.5 eV, respectively. By comparison, the L-edge features of vanadium carbide are substantially broadened. A similar broadening effect was observed by comparing powder materials of VC and metallic vanadium.[43] One possible explanation is that the width of the unfilled d band is broadened significantly after carbide formation. This would make it a rather poorly defined final state for the p → d transitions, resulting in a broadening in the L-edge features in the NEXAFS measurements. For comparison, Figure 11b also shows the Mo M-edge features of clean and carbide-modified Mo(110). The experimental conditions were the same as those used for Figure 10b. Again, the M-edge features, which involve the transitions of 3p electrons to the unfilled states of the Mo 4d band, are somewhat broadened on the carbide-modified surface. It is also interesting to notice that the degree of broadening is less than that observed for the vanadium carbide overlayer (Figure 11a).

3. Chemisorption of CO on Carbide Surfaces

In this section we will use the chemisorption of CO molecules to further illustrate the difference between the electronic properties of metal carbides and those of their parent metals.

The chemisorption and decomposition of CO molecules on transition metal surfaces have been extensively investigated and have been the subject of several comprehensive review articles.[138−141] In brief, CO molecules interact with metal surfaces via two parallel mechanisms: (1) donation from the 5σ orbital of CO into metal surface orbitals of appropriate symmetry (primarily d_{z^2}) and (2) donation from the metal d orbitals of appropriate symmetry (primarily d_{xz} and d_{yz}) into the $2\pi^*$ antibonding orbitals of CO. The 5σ donation can occur without a significant weakening of the CO bond. However, the back-donation to the $2\pi^*$ antibonding orbitals can substantially weaken the C−O bond while strengthen the metal−carbon bond. In general, CO molecules interact strongly with clean surfaces of groups IVB−VIB metals, leading to the decomposition of CO molecules. On the other hand, the interaction of CO with low-index surfaces of group VIII metals (except Fe and Co) is weaker, with chemisorbed CO desorbing molecularly intact from the surfaces at higher temperatures.

Theoretical investigations of the interaction of CO with TiC(100), TiC(111), and clean Ti(0001) surfaces have been carried out by Jansen and Hoffmann, using the extended Hückel tight-binding method.[23]

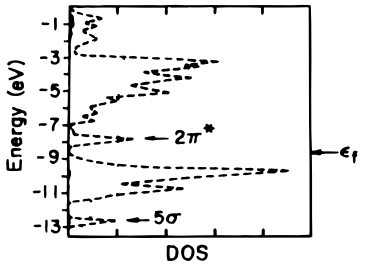

Figure 12. An example of the extended Hückel calculations of the projected DOS of CO+TiC(100). (Reprinted from ref 23. Copyright 1988 Elsevier.)

Table 2. Extended Hückel Calculations of the Occupation of the 5σ and 2π* Molecular Orbitals of CO on Different Surfaces (Reprinted from ref 23. Copyright 1988 Elsevier.)

	free CO	Ti(0001)	TiC(100)	TiC(111)	$TiC(100)_{0.5}$[a]
5σ	2	1.730	1.725	1.727	1.725
2π[a]	0	1.610	0.132	1.430	1.380

[a] TiC(100) surface with 50% carbon deficiency.

As discussed earlier in section 2.3 (see Figure 2), the (100) surface of TiC is characterized by the coexistence of both Ti and C, while the (111) surface has alternative layers of Ti and C . Figure 12 shows an example of the projected DOS for the composite of TiC(100) + CO.[23] The two CO molecular orbitals are labeled as 5σ and 2π*, which appear at the relative energy scales of −12.5 and −7.8 eV, respectively. The remaining orbitals are related to the TiC(100) substrate. In brief, the doublet feature in the relative energy range of −9 to −12 eV is related primarily to the C 2p and the set of multiple features at −3 to −7 eV is related mainly to the Ti 3d orbitals. Qualitatively, Figure 12 shows that the degree of interaction, as judged by the overlapping of molecular orbitals of CO with those of the TiC(100) surface, is small.[23]

From these theoretical studies, Jansen and Hoffmann were able to observe the different degrees of interaction of CO on Ti(0001) and various TiC surfaces by calculating the occupation of the 5σ and 2π* orbitals of CO, the medium energy of the 2π* orbital, and the overlap population of the C−O and metal−carbon orbitals.[23] For example, Table 2 shows a comparison of the occupation of the 5σ and 2π* orbitals of CO. For free CO molecules, the occupation of these two orbitals is 2 and 0, respectively. For adsorbed CO molecules, the occupation of the 2π* orbital is determined by the amount of charge donation from the substrate, which is directly related to the degree of interaction between CO and the substrate. The relatively weak interaction of CO with the TiC(100) surface is characterized by the small degree of occupation of the 2π* antibonding orbitals of CO, namely 0.132. This number is substantially less than that on clean Ti(0001), which is calculated to be 1.610.[23] Table 2 also illustrates the significant difference in the interaction of CO with the TiC(100) and TiC(111) surfaces, with the latter being characterized by a 2π* occupation of 1.430. This is in excellent agreement with the experimentally observed differences in the reactivities of the TiC(100) and TiC(111) surfaces.[34,35] Finally, Table 2 also demonstrates the importance of surface defects, or

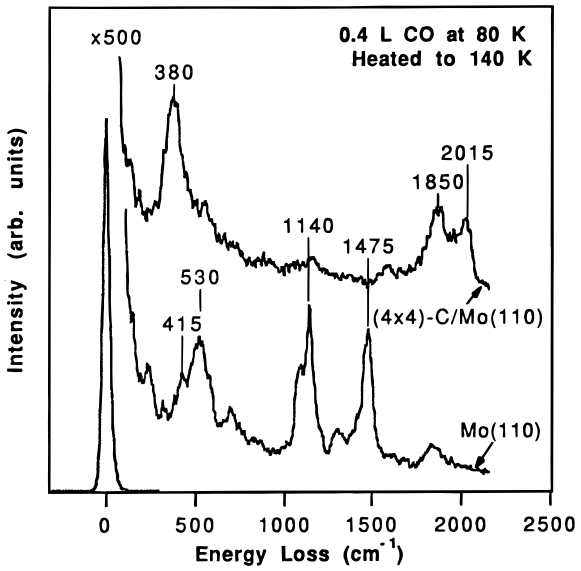

Figure 13. HREELS spectra of CO adsorption on Mo(110) and (4×4)-C/Mo(110). The adsorbed layers were prepared by exposing submonolayer coverage (0.4 L) of CO at 80 K followed by heating to 140 K. (Reprinted from ref 59. Copyright 1995 Elsevier.)

the so-called "carbon deficiency", of the carbide surface. The last column in Table 2 represents the orbital occupation of CO molecules on a TiC(100) surface with a 50% carbon deficiency. The reactivity of TiC(100) is enhanced as a result of carbon deficiency, with the occupation of the 2π* orbitals of CO increasing from 0.132 on the perfectly oriented TiC-(100) surface to 1.380 on the carbon deficient TiC-(100) surface.[23]

By comparing the theoretical results of CO on Ti-(0001) and TiC(100) surfaces, it is clear that CO molecules interact differently with the clean surface and the carbide surface with coexisting C and Ti atoms. One of the primary reasons for the reduced reactivity of the carbide surface is the reduction in the ability of this substrate to donate electrons into the 2π* antibonding orbitals of CO. Similar behavior has been observed experimentally in the comparative studies of CO on clean and carbide-modified surfaces of V(110),[44] Mo(100),[49] Mo(110),[59] and W(100).[71] One general observation from these studies is that the interaction of CO molecules changes from dissociative adsorption on the clean surfaces to reversible chemisorption on the carbide modified surfaces.

For example, Figure 13 shows a comparison of HREELS spectra of CO molecules on clean Mo(110) and on a (4×4)-C/Mo(110) overlayer. The clean Mo-(110) surface interacts very strongly with CO molecules, as indicated by the observation of CO species with unusually low ν(CO) vibrational frequencies at 1140 and 1475 cm^{-1}. These vibrational frequencies are substantially lower than the gas-phase ν(CO) value of 2143 cm^{-1}.[142] These two low-frequency features are assigned to CO molecules bonding to the surface in the parallel and inclined configurations, respectively.[143] The fact that CO species adopt the parallel and inclined orientations, instead of the conventional perpendicular configurations, has been attributed to the strong d−2π* interaction between the clean Mo surface and CO molecules.[143] These

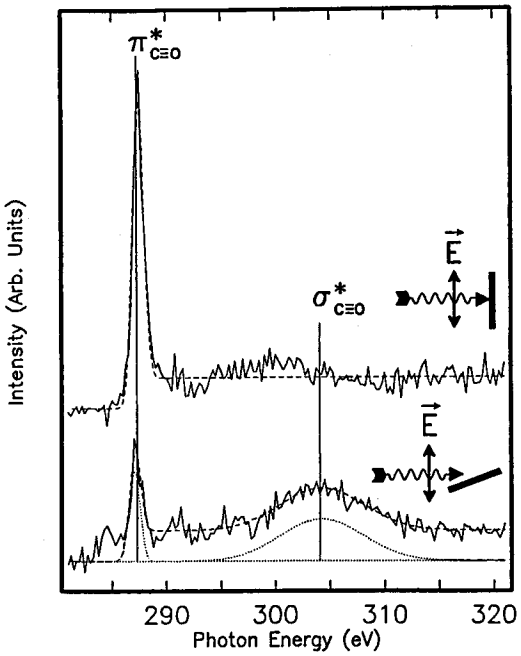

Figure 14. Polarization dependent NEXAFS of CO on (5×1)-C/W(100). (Reprinted from ref 71. Copyright 1987 American Institute of Physics.)

strongly bonded CO species eventually dissociate at higher temperatures, as observed in the HREELS and TPD measurements.[59,144] On the other hand, the interaction is much weaker for CO species adsorbed on the (4×4)-C/Mo(110) surface. The primary CO species on the carbide-modified surface are the perpendicularly bonded CO molecules in the terminal (2015 cm^{-1}) and bridging (1850 cm^{-1}) configurations.[59] Upon heating the surface, these perpendicularly bonded CO species desorb molecularly intact, supporting the argument of a weaker d−2π* interaction between CO and the carbide-modified surface.

Finally, the weaker interaction between CO molecules and carbide modified-surfaces was also confirmed by the polarization dependence NEXAFS studies of CO on the (5×1)-C/Mo(100) surface,[71] as shown in Figure 14. The orientation of the adsorbed CO molecules can be derived from the polarization dependence of the π* and σ* resonances, which are perpendicular and parallel to the CO molecular axis, respectively.[71,84] From the polarization dependence of the π* and σ* resonances,[71,84] the C−O bond orientation was estimated to be 90 ± 5° with respect to the surface direction of (5×1)-C/Mo(100). This observation again confirms that the adsorption of CO on the carbide-modified surfaces takes the less interactive perpendicular orientation. Furthermore, the weak interaction between adsorbed CO and the (5×1)-C/W(100) surface was also evident from the value of the C−O bond length, which could be estimated from the peak positions of the σ* resonance.[71,84] The C−O bond length on (5×1)-C/W(100) was estimated to be 1.12 + 0.03 Å, which was very close to the bond length of a free CO molecule of 1.128 Å.[142,145] Again, the lack of modification on the C−O bond length is the direct consequence of the very weak interaction between CO and the carbide modified surface.

V. Surface Reactivities of Carbide and Nitride Overlayers

Surface reactivities of carbide overlayers on V(110), Mo(100), Mo(110), and W(100) and nitride overlayers on Mo(100) and Mo(110) have been the subject of many investigations. We will use these modified surfaces to review the surface reactivities of carbide/nitride overlayers. We will concentrate on two important issues related to the surface reactivities of carbide and nitride overlayers: (1) the difference between carbide/nitride-modified surfaces from their parent metals and (2) the similarities and/or differences among various carbide- and nitride-modified surfaces. We will start this section by reviewing the systematic trends in the reactivities of carbide and nitride overlayers toward several classes of organic molecules. The general similarities and differences in the surface reactivities will be summarized at the end of this section.

1. Reactions with Saturated and Unsaturated Hydrocarbons

1.1. Reactions with Ethylene: New Surface Intermediates

The adsorption and decomposition of ethylene molecules are commonly used to compare the reactivities of different metal surfaces in both experimental and theoretical investigations. The reaction pathway of ethylene is often distinct from one group of metals to the other. The interaction of the C=C bond of ethylene with transition metals has been often described by the Chatt−Dewar−Duncanson mechanism, which involves primarily the donation−back-donation of π electrons of ethylene and d electrons of metals.[148] In this mechanism, electrons in the highest filled π orbital of ethylene are partially donated to an empty σ orbital of the metal atom. Such a donation weakens the π bond of ethylene and lowers the energy level of the lowest lying antibonding π* orbital, which in turn allows a more efficient back-donation of electrons from the metal atom, further weakening the C=C bond. A more detailed description was given in a recent quantum calculation of the bonding of ethylene with the second-row transition metals.[148] In their paper, Blomberg et al. have investigated the activation mechanisms of the C=C bond of ethylene for the entire second-row transition metals and have observed a general trend in the reactivities from the left side to the right side of the periodic table.[148] They proposed several different types of bonding configurations between the C=C bond and the metal atom, depending on the location of the metal in the periodic table. For those metals on the left side of the periodic table, a covalent bond is predicted between ethylene and the metal, in which the π bond of ethylene is effectively broken and a metallacyclopropane is produced. The carbon−carbon bond length in this complex is estimated to be in the range of 1.51−1.54 Å, which can be best described as a C−C single bond. On the other hand, for those metals on the right side of the periodic table (group VIII), the bonding is considered to be a compromise between the covalent and donation−back-donation forms of bonding. The carbon−carbon bond distance is roughly in between that of a double

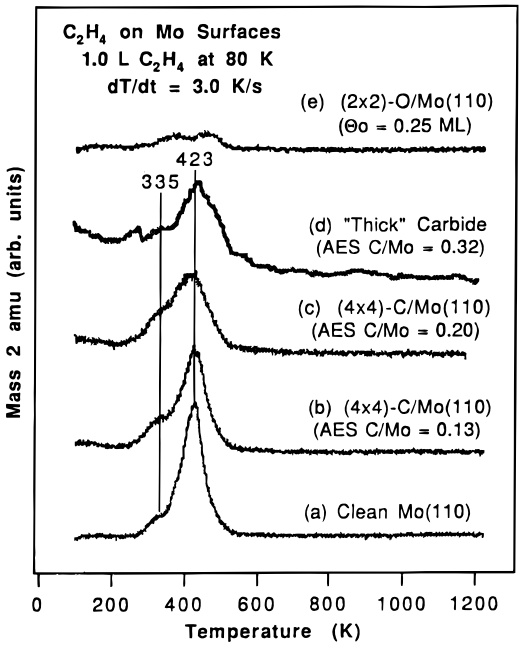

Figure 15. Comparison of TPD spectra of H_2 after the reaction of submonolayer coverage (1.0 L) of ethylene with clean and carbide-modified Mo(110). (Reprinted from ref 59. Copyright 1995 Elsevier.)

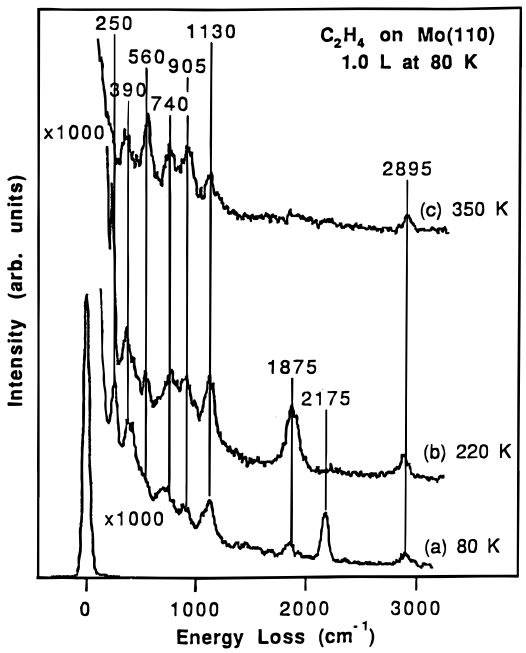

Figure 16. HREELS spectra following the thermal decomposition of submonolayer coverage (1.0 L) ethylene on clean Mo(110). The vibrational features at 1875 and 2175 cm^{-1} are due to background adsorption of CO and N_2, respectively. These impurities, collected during either ethylene dosing or data acquisition, are estimated to be less than 0.05 ML on the surface. (From ref 147.)

and a single bond, indicating a relatively weaker interaction between the C═C bond and the group VIII metals.

These theoretically predicted reactivities agree with the experimentally observed reactivities of ethylene on different metal surfaces. For example, on groups IVB−VIB early transition metals, ethylene undergoes complete decomposition to produce atomic carbon and hydrogen, while on Pt group metals (Ru, Os, Rh, Ir, Pd, Pt) ethylene decomposes via an ethylidyne (CCH_3) intermediate.[146] Therefore, comparative investigations of the degree of decomposition and reaction pathways of ethylene on carbide/nitride overlayers and their parent metals[44,48,59,72,147] would answer two important questions: (1) how are the reactivities of these overlayers different from their parent metals and (2) what are the similarities between the reactivities of these overlayers with Pt group noble metals.

Comparative investigations of the reactivities of ethylene on carbide overlayers and on the corresponding parent metals have been carried out on V(110),[44] Mo(100),[48] Mo(110),[59,147] and W(100).[70] Figure 15 shows a comparison of thermal desorption of H_2 after the reaction of ethylene on Mo(110) and on several carbide-modified surfaces.[59] At low coverages on clean Mo(110), ethylene undergoes complete decomposition to produce atomic carbon and hydrogen, the latter recombines to desorb as H_2. The gas-phase decomposition products are H_2 on all surfaces; the peak areas of hydrogen desorption in Figure 15 can therefore be used as an indication of the degree of ethylene decomposition on these surfaces. The carbide-modified surfaces in Figure 15 were prepared by exposing Mo(110) to ethylene at $T \leq 600$ K followed by annealing the surface to 1200 K (see Figure 9). The "thick" carbide (Figure 15d) was prepared by repeated cycles of dosing and annealing. For comparison, the TPD spectrum from an oxygen-modified Mo(110) with a coverage of 0.25 ML (monolayer) is also shown in Figure 15e. A simple comparison of the H_2 peak areas in Figure 15 indicates that both the clean and the carbide-modified Mo(110) surfaces are reactive toward the decomposition of ethylene, whereas the reactivity is nearly suppressed by the presence of only 0.25 ML of surface oxygen. Although the H_2 desorption peak becomes broad on carbide modified surfaces, the changes in the relative peak areas of H_2 are small when going from clean to carbide-modified surfaces with increasing C/Mo ratios.

The corresponding HREELS measurements of reactions of ethylene on Mo(110) and (4×4)-C/Mo(110) indicated that the reaction pathways are different on the two surfaces.[147] Figure 16 shows a set of HREELS spectra following the thermal behavior of ethylene on clean Mo(110). As expected, ethylene interacts very strongly with clean Mo(110) even at 80 K. In fact, by comparing Figure 16a with literature data and by studying the isotope shift with C_2D_4 on Mo(110),[147] the HREELS spectrum at 80 K can be best described as an acetylene-like species. This observation clearly indicates the very strong interaction between ethylene and Mo(110), leading to the decomposition of the C−H bonds of ethylene at temperatures as low as 80 K. The vibrational features in Figure 16a can all be assigned to acetylene species:[147] a ν(C−H) mode at 2879 cm^{-1}, a ν(C−C) mode at 1130 cm^{-1}, an in-plane CH bend at 905 cm^{-1}, an out-of-plane bend at 740 cm^{-1}, a ν(Mo−C) mode at 390 cm^{-1}, and a surface phonon mode at 250 cm^{-1}. As shown in Figure 16, the acetylene species are stable up to 350 K. At higher temperatures they decompose to produce gas-phase H_2 (Figure 15) and atomic carbon; no other intermediates were detected in the

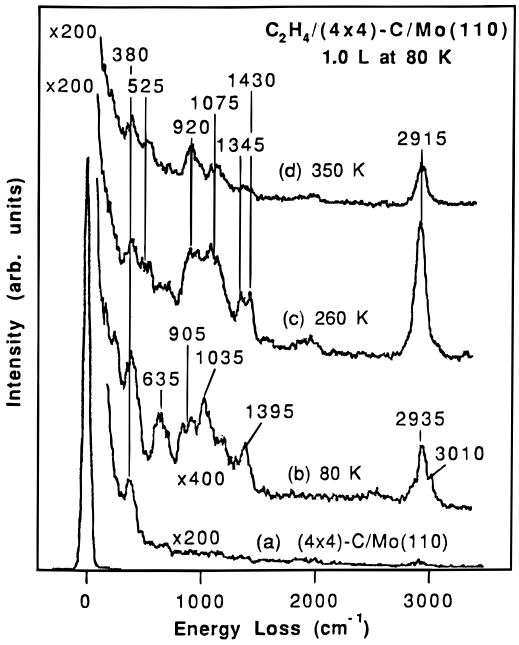

Figure 17. HREELS spectra following the thermal decomposition of submonolayer coverage (1.0 L) of ethylene on (4×4)-C/Mo(110). (From ref 147.)

HREELS measurements.[147]

The decomposition mechanism of ethylene on the (4×4)-C/Mo(110) surface is significantly different. HREELS spectra following the thermal decomposition of ethylene on (4×4)-C/Mo(110) are compared in Figure 17. The first major difference is that ethylene does not decompose on this surface at 80 K. The HREELS spectrum in Figure 17b is typical for ethylene species adsorbed in the di-σ configuration, as commonly observed on group VIII metal surfaces.[147] The vibrational assignments are confirmed by comparing Figure 17b with literature data and by studying the isotope shift with C_2D_4 on (4×4)-C/Mo(110).[147] In brief, the 3010 and 2935 cm^{-1} features are due to the asymmetric and symmetric $\nu(CH_2)$ modes, respectively; the 1395, 1035, 905, and 635 cm^{-1} modes are due to the CH_2-scissor, CH_2-wag, CH_2-twist, and CH_2 out-of-plane bend, respectively; and the mode at 1035 cm^{-1} is primarily related to the ν(C−C) motion. The observation that ethylene molecules remain intact on the (4×4)-C/Mo(110) surface at 80 K indicates that this surface is much less reactive than the clean Mo(110) surface.

Another important difference for the reaction of ethylene on the (4×4)-C/Mo(110) surface is that a new intermediate is produced at 260 K, as shown in Figure 17c. The number of vibrational features and their relative intensities indicate that this species is neither acetylene (Figure 16a) nor di-σ-bonded ethylene (Figure 17b). The vibrational spectrum can be best described as that of an ethylidyne species (CCH_3). The vibrational assignment is compared in Table 3 to those of ethylidyne species on Pt(111)[149] and in an organometallic compound.[150] The most characteristic ethylidyne features in Figure 17c are those related to the terminal CH_3 group, i.e., the relatively intense $\nu_s(CH_3)$, $\delta_{as}(CH_3)$, and $\delta_s(CH_3)$ modes at 2915, 1430, and 1345 cm^{-1}, respectively.[147] Ethylidyne species were also detected on the carbide-modified V(110) surface.[44] Because the formation of ethylidyne species is exclusively observed on the clean surfaces of Pt group metals, the detection of this species on the carbide overlayers of groups VB−VIB metals therefore provides an example for the general similarities between the surface reactivities of early transition metal carbides and noble metals. It is also important to point out that thermal stability of ethylidyne species is different on the carbide and Pt group metal surfaces. While ethylidyne species start to decompose on the former surface at $T \geq 400$ K, they are stable on some of the Pt group metal surfaces at temperatures as high as 650 K.

The results shown in Figures 15−17 demonstrate that the decomposition mechanisms of ethylene are qualitatively different on Mo(110) and on carbide modified Mo(110), although the degree of decomposition, as judged from TPD results, is nearly the same on the two types of surfaces. The latter observation is somewhat different from ethylene reactions on carbide-modified Mo(100)[48] and W(100),[72] which concluded that the degree of ethylene decomposition on the carbide-modified surfaces was significantly lower than on the clean surfaces. One possible explanation would be that the surface concentration, as well as the location of carbon atoms, might be different for the different carbides overlayers. Figure 18 shows an example of the importance of the surface concentration and/or the location of carbon atoms in determining the reactivity of carbide overlayers toward ethylene. The preparation procedures of the two carbide overlayers in Figure 18 were described earlier (see Figure 9). The unannealed carbide overlayer (a) was prepared by exposing Mo(110) to 4.0 L of ethylene at 600 K without annealing to higher temperatures. The annealed carbide overlayer (b) was prepared by five cycles of doing 300 L of ethylene at 600 K followed by annealing to 1150 K. Both surfaces were characterized by an AES C(KLL)/Mo(MNN) ratio of 0.3, suggesting a similar carbon concentration

Table 3. Vibrational Assignments of Ethylidyne Species on Different Surfaces

vibrational assignment	C_2H_4 (C_2D_4) on Pt(111) $\xrightarrow{\Delta}$ 415 K[a]	ω_H/ω_D	$(CH_3C)Co_3(CO)_9$ ($(CD_3C)Co_3(CO)_9$) (IR and calculations)[b]	ω_H/ω_D	C_2H_4 (C_2D_4) on (4×4)-C/Mo(110) $\xrightarrow{\Delta}$ 260 K[c]	ω_H/ω_D
ν-MC (s)	430 (410)	1.05	401 (393)	1.02	380 (−)	−
ν-MC (as)	600 (600)	1.00	555 (536)	1.04	525 (560)	0.94
ρ-CH_3	980 (790)	1.21	1004 (828)	1.21	920 (670)	1.37
δ-CH_3 (s)	1350 (990)	1.36	1356 (993)	1.37	1345 (1015)	1.33
δ-CH_3 (as)	1420 (1030)	1.38	1420 (1031)	1.38	1420 (−)	−
ν-CC	1130 (1160)	0.98	1163 (1182)	0.98	1075 (1105)	0.97
ν-CH_3 (s)	2890 (2080)	1.39	2888 (−)	−	2915 (2180)	1.34
ν-CH_3 (as)	2950 (2220)	1.33	2930 (2192)	1.34	− (−)	−

[a] Reference 149. [b] Reference 150. [c] Reference 147.

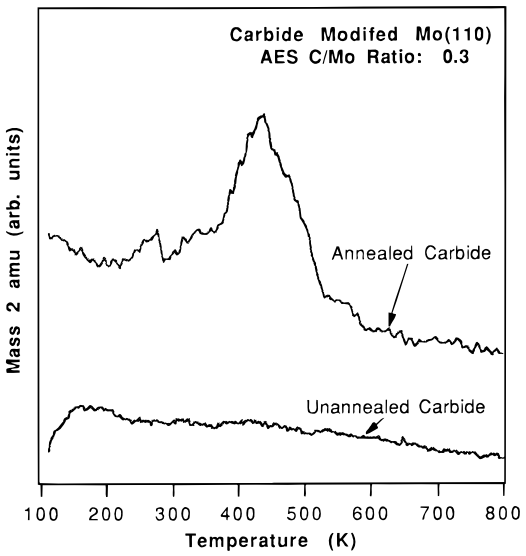

Figure 18. Comparison of TPD spectra of H_2 after the reaction of ethylene with an unannealed and annealed carbide overlayers on Mo(110). Both carbide modified surfaces are characterized by an AES C(KLL)/Mo(MNN) ratio of 0.3. (Reprinted from ref 60. Copyright.)

within the AES sampling depth. As expected, NEXAFS measurements using fluorescence−yield shows a greater abundance of subsurface carbon for the latter surface.[60] As shown in Figure 18, the decomposition of ethylene is completely suppressed on the unannealed carbide overlayer, while the decomposition occurs readily on the annealed carbide surface. It is most likely that the carbon atoms stay primarily on the surface of the unannealed carbide overlayer, blocking the surface sites necessary for the decomposition of ethylene. For the annealed carbide overlayer, the number of carbon atoms occupying the surface sites might be much less due to the thermally induced diffusion process (see Figure 9). This observation is also likely related to the carbon deficiency on the annealed C/Mo(110) surface, as discussed in section 4.3 for the different reactivities of the perfectly oriented and the carbon-deficient TiC(100) surfaces.[23] The comparison in Figure 18 clearly indicates that a detailed understanding of the surface structures, as well as the local carbon/metal stoichiometrics, is essential when the reactivities of different carbide overlayers are compared. The reaction of ethylene on nitride-modified Mo(110) was also investigated.[60] Results from TPD and HREELS measurements suggest that nitrogen plays a simple site-blocking role. Unlike the new decomposition mechanism observed on the carbide modified surface, the presence of nitrogen atoms on Mo(110) simply blocks the decomposition of ethylene, in the similar fashion as the unannealed carbide surface. More about the site-blocking mechanism of nitrogen on Mo(110) will be discussed later.

1.2. Reactions with Cyclic Hydrocarbons: New Reaction Products

Reactions of cyclic hydrocarbons with carbide overlayers provide examples of the production of gas-phase reaction products that are different from those on the clean parent metals. Figure 19 shows a comparison of the thermal desorption of cyclohexene (A), H_2 (B), and benzene (C) after the reaction of cyclohexene with clean and several chemically modified Mo(110) surfaces.[151] As shown in Figure 19A, cyclohexene adsorbs irreversibly on the clean Mo(110) surface, leading to the complete decomposition to atomic carbon and hydrogen. The only gas-phase decomposition product is H_2 (Figure 19B). Cyclohexene also adsorbs irreversibly on the (4×4)-C/Mo(110) surface.[151] However, it undergoes partial dehydrogenation instead of complete decomposition, as indicated by the detection of benzene as a reaction product (Figure 19C). The combined HREELS and TPD investigations indicated that the desorption of benzene is reaction limited on the (4×4)-C/Mo(110) surface at temperatures ≥ 300 K.[151] Overall, the reaction pathways of cyclohexene (c-C_6H_{10}) on Mo(110) and (4×4)-C/Mo(110) are different:

$$\text{on Mo(110)} \qquad \text{c-}C_6H_{10} \rightarrow 6C_{(a)} + 5H_2\,(g)$$

$$\text{on (4}\times\text{4)}-\text{C/Mo(110)} \qquad \text{c-}C_6H_{10} \rightarrow C_6H_6\,(g) + 2H_2\,(g)$$

It is interesting to point out that the primary reaction mechanism of cyclohexene on noble metals, such as Pt(111),[152] is also via the partial dehydrogenation to produce benzene. This example again demonstrates the general similarity between the reactivities of carbide overlayers and noble metals.

Figure 19 also shows that unlike the carbide-modified surface, benzene is not produced on the nitride-modified Mo(110) surface. In fact, the adsorption of cyclohexene is reversible on both nitride- and oxygen-modified Mo(110), as indicated by the strong molecular desorption peak at ~220 K (Figure 19A), and by the absence of H_2 (Figure 19B) or benzene (Figure 19C) as decomposition products. The relatively weak and sharp benzene TPD peaks at 220 K on both nitride- and oxygen-modified Mo(110) are due to the molecular desorption of cyclohexene, because mass 78 amu (benzene) is also a minor cracking product of cyclohexene. The difference between the reaction of cyclohexene with carbide and nitride-modified Mo(110) is also demonstrated in the HREELS measurements following the adsorption of cyclohexene at 150 K,[151] which are shown in Figure 20. Even without going into detailed vibrational assignments,[151] it is clear that the interaction of cyclohexene on the nitride- and oxygen-modified surfaces is very weak, as indicated by the detection of the δ(C═C) mode at 720 cm^{-1} and the ν(C═C) mode at 1600 cm^{-1}, indicating that the C═C bond of cyclohexene is unperturbed due to the lack of interaction between the adsorbate and the substrate. This is clearly not the case on either clean Mo(110) or on (4×4)-C/Mo(110). Vibrational features related to the C═C bond motions are absent on these two surfaces, since the C═C bonds become sp^3 in nature due to the strong d−σ interaction between the adsorbate and the substrate. Therefore, the HREELS results confirm the TPD data that cyclohexene reacts strongly on Mo(110) and C/Mo(110), while it interacts very weakly on the nitride- and oxygen-modified surfaces.

The difference in the reactivities of carbide- and nitride-modified Mo(110) surfaces is very intriguing,

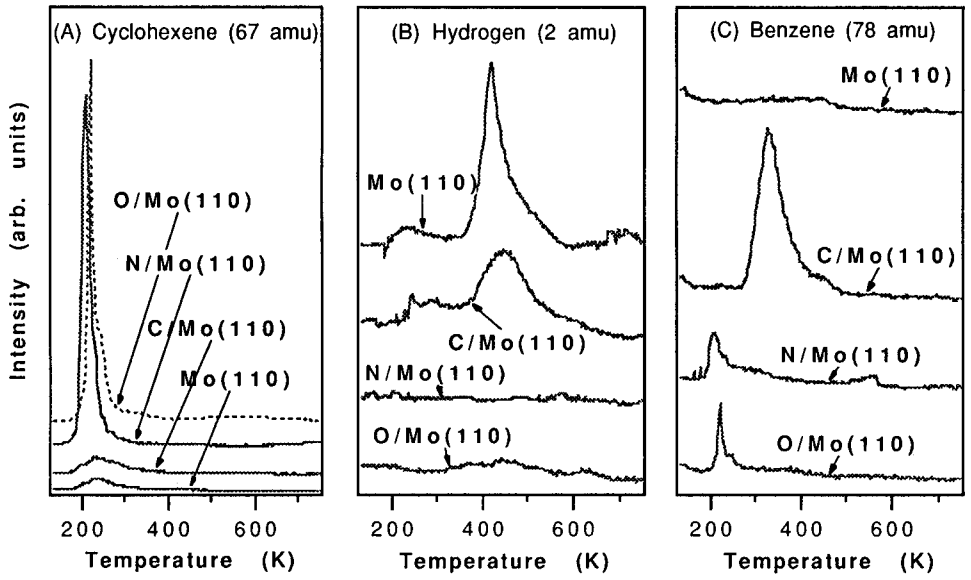

Figure 19. Thermal desorption of (A) cyclohexene, (B) hydrogen, and (C) benzene after reactions of submonolayer coverage (3.0 L) of cyclohexene with Mo(110), C/Mo(110), N/Mo(110), and O/Mo(110). (From ref 151.)

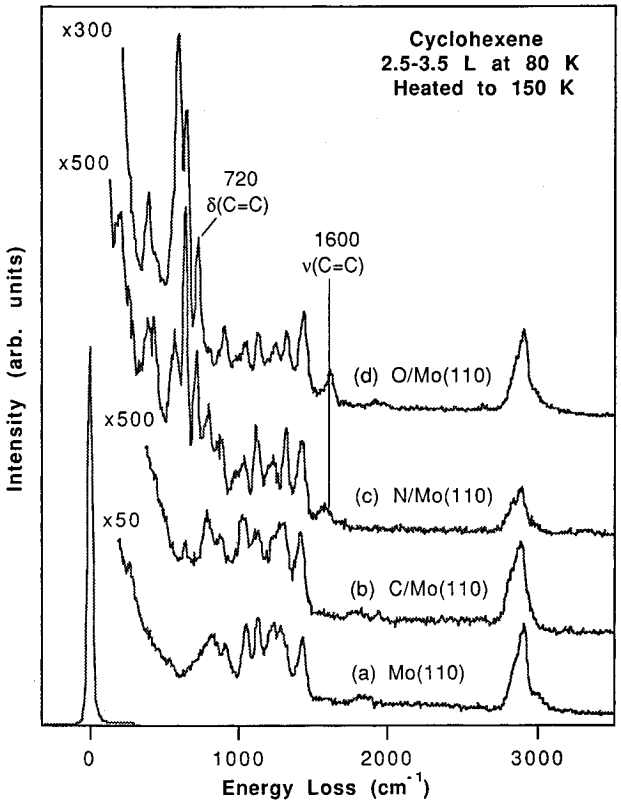

Figure 20. HREELS spectra after the adsorption of submonolayer coverage of cyclohexene on different Mo(110) surfaces. The adsorbed layers were prepared by dosing 3.0 L cyclohexene at 80 K followed by heating to 150 K. (From ref 151.)

especially by considering the fact that the catalytic properties of bulk Mo_2C and Mo_2N are nearly identical.[2] This might be explained by the different surface concentrations and/or adatom locations of the two overlayers, as discussed earlier (see Figure 9). Unlike the carbide overlayer, the nitride-modified surface is most likely characterized by nitrogen atoms occupying the surface sites. The thermally induced diffusion of nitrogen into the subsurface/interstitial sites, which is essential for modeling the chemistry of bulk nitride, can not be achieved on the nitride-modified Mo(110) since the competitive recombination reaction prevails. This would also explain the similarity between the nitride-modified and oxygen-modified surfaces. The latter surface is characterized by 0.25 ML of oxygen atoms occupying only the surface sites without any bulk diffusion. In general, these electronegative oxygen atoms reduce the surface reactivities of groups IVB−VIII transition metals by the following two mechanisms: (1) occupation of the reactive sites by site-blocking and (2) withdrawing and localizing the surface electron density. As a result, the oxygen-modified surface becomes less or nonreactive toward the adsorbed molecules with unsaturated bonds. The inert nature of the nitride-modified Mo(110) and its apparent similarity with the oxygen-modified Mo(110) suggest that nitrogen atoms reduce the surface reactivity in a similar way as oxygen atoms. It is obvious from Figures 19 and 20 that the nitride-modified Mo(110) cannot be used as a reliable model for the bulk nitride catalysts, because of the inability to produce nitrogen atoms occupying the subsurface/interstitial sites. As discussed for the different reactivities of the unannealed (surface carbon) and annealed (interstitial carbon) C/Mo(110),[60] nitride overlayers with interstitial nitrogen atoms should also show reactivities characteristic of bulk nitrides. Detailed reactivity studies of hydrocarbon molecules on these overlayers, such as the (1×1)-N/Ti(0001) surface,[101,102] should provide important information on the similarities and/or differences of the surface reactivities of carbide and nitride overlayers. Nitride overlayers prepared under other experimental conditions, such as the ion beam-assisted deposition (IBAD) deposition of thin nitride films,[128−130] should also be used as model systems to understand the surface reactivities of nitride overlayers.

Reactions of carbide overlayers with other cyclic molecules, such as cyclopropane,[55] cyclohexane,[151] cyclohexadiene,[151] benzene,[153] and cycloheptatriene[70] have also been investigated. The latter study reported that different gas-phase products were de-

tected after the reaction of cycloheptatriene with clean and carbide-modified W(100).[70] For example, on clean W(100), cycloheptatriene undergoes complete decomposition to produce atomic carbon and hydrogen, with the latter recombining to produce H_2 at higher temperatures. On the (5×1)-C/W(100) surface, however, the primary decomposition product was found to be benzene.[70] Not surprisingly, the analogous decomposition pathway of cycloheptatriene on (5×1)-C/W(100) was observed on the surface of one of the Group VIII metals, Ni(100).[154] This study again demonstrates that the very strong reactivities of early transition metals can be "tamed" by the formation of carbide, and the reactivities of the carbide overlayers are generally similar to those of group VIII metals.

1.3. Reactions with C4 Hydrocarbons: Activation of C−H and C═C Bonds

The results presented above demonstrate that the reactivities of carbide overlayers toward unsaturated hydrocarbons are reduced as compared to their parent metals. This is reflected either by a decrease in the amount of molecules undergoing dissociation or by a modified reaction pathway that favors partial decomposition over the complete decomposition to atomic carbon and hydrogen. Similar to that discussed earlier for the interaction of carbide with CO molecules (section 4.3), the weaker interaction can be primarily related to the reduction in the ability of carbides to donate d electrons to the π^* antibonding orbital of the C═C bond. A similar trend has been observed for the reactions of carbide overlayers with unsaturated C4 hydrocarbons, such as 1-butene, 2-butene, isobutene, and 1,3-butadiene molecules.[43,45,54]

Attempts to understand the activation of C−H bonds of saturated hydrocarbons and C═C bonds of unsaturated molecules have been carried out on carbide-modified surfaces of V(110),[43,45] Mo(100),[54] and Mo(110).[155] Figure 21 shows a comparison of H_2 desorption after reactions of 1,3-butadiene (A) and *n*-butane (B) on clean and carbide-modified V(110) surfaces.[45] These two molecules were chosen as model systems for the activation of C═C and C−H bonds because their carbon atoms are completely sp^2- and sp^3-hybridized, respectively. As shown in Figure 21A, the degree of 1,3-butadiene decomposition, as judged from the relative peak areas of H_2, decreased significantly on the carbide-modified surfaces. The carbide surface designated as 1.0 C/V was characterized by a stoichiometry of VC from AES measurements, and the average carbide overlayer thickness was estimated to be ≥10 Å from NEXAFS measurements.[46] Using a combination of AES and TPD, the degree of 1,3-butadiene decomposition was estimated to be 0.18 ML on V(110) and 0.04 ML on VC/V(110). On the other hand, as shown in Figure 21B, the degree of *n*-butane dissociation increases from V(110) to VC/V(110). The amount of *n*-butane dissociation on the two surfaces was estimated to be 0.01 and 0.07 ML, respectively.[45] Similar enhancement in the activation of C−H bonds has been observed for the dissociation of isobutane on VC/V(110).[43]

The results shown in Figures 21 suggest that VC/V(110) should be much more effective for the dehydrogenation of saturated hydrocarbons than clean V(110). This is because the carbide overlayer shows an enhancement in the activation of the C−H bond of saturated hydrocarbons (reactants in dehydrogenation reactions) and a decrease in the reactivity toward the C═C bond of unsaturated molecules (products in dehydrogenation reactions). This has been observed for the dehydrogenation of isobutane to isobutene on powder materials of vanadium and vanadium carbide.[43] For example, the dehydrogenation activities of isobutane over vanadium and vanadium carbide powder catalysts are compared in Figure 22. Compared to vanadium, VC catalysts show a higher rate for isobutane conversion (A) and a better selectivity for isobutene in the product distribution (B).[43] These results clearly support the surface science observations of an enhancement in the activation of the C−H bond of saturated hydrocarbons on the carbide-modified V(110) surface.

One possible explanation for the enhancement of C−H bond activation on VC/V(110) has been suggested to be related to the electronic structures of vanadium carbide above the Fermi level.[45] Results from IPE measurements of bulk VC crystals reveal the presence of various unfilled states near the Fermi level.[6] As mentioned earlier, the DOS of unfilled states of the vanadium d band is most likely broad-

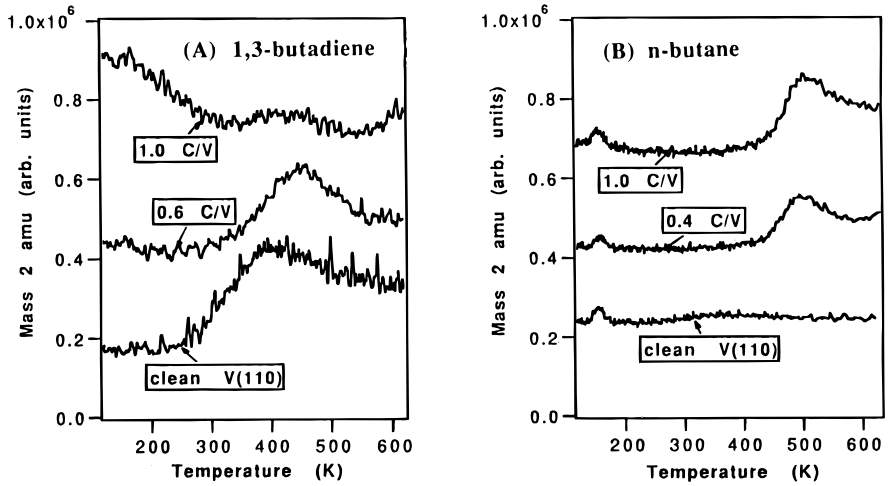

Figure 21. Thermal desorption of H_2 after reactions of submonolayer coverages of (A) 1,3-butadiene and (B) *n*-butane with clean and carbide-modified V(110) surfaces. (Reprinted from ref 45. Copyright 1995 Academic.)

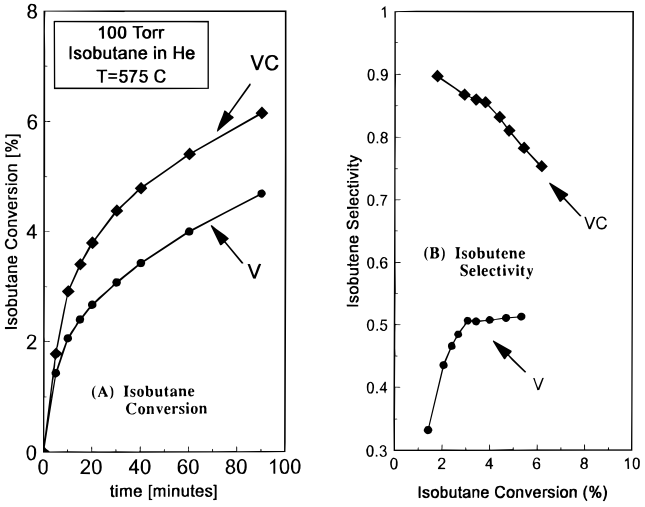

Figure 22. Dehydrogenation of isobutane to isobutene on V and VC powder catalysts in a batch reactor. The isobutane conversion rate (A) was normalized to the surface areas of the catalysts. The isobutene selectivity (B) was normalized by the total reaction products. The formation of carbide on the metallic vanadium catalysts, during the dehydrogenation reaction, is also suggested by the gradual increase in the isobutene selectivity. (Reprinted from ref 43. Copyright 1996 Blackie Academic and Professional.)

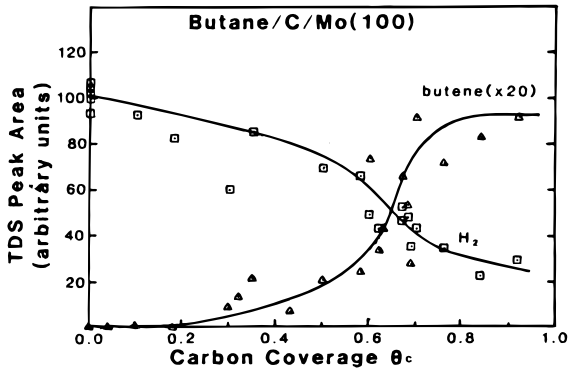

Figure 23. Thermal desorption of H_2 and 1-butene following the reaction of *n*-butane on carbide-modified Mo(100). (Reprinted from ref 54. Copyright 1986 Elsevier.)

ened after the formation of carbide (Figure 11a). The C−H bond of alkanes can be weakened when it is bonded in the three-center, agostic bonding model,[156] which involves the donation of the electron pair of the C−H bond to a vacant orbital on the metal center. The availability of the broad, unoccupied orbitals on the vanadium carbide surface should therefore enhance the probability for the activation of C−H bonds of alkanes. However, more detailed experimental and theoretical band structure investigations are needed for an overall understanding of the relationship between the electronic properties of carbides and the activation mechanisms of C−H bonds on these surfaces.

The enhancement in the activation of *n*-butane was not observed on carbide-modified Mo surfaces. The dissociation of *n*-butane was found to occur on both clean and carbide-modified Mo(100) surfaces, and the amount of decomposition was observed to be ~0.05 ML on both surfaces.[54] However, the presence of carbide alters the decomposition products of *n*-butane. As shown in Figure 23, the decomposition product is primarily H_2 on clean Mo(100) and on carbide-modified surfaces with low carbon concentrations. The dominant decomposition product becomes butene as the surface carbon concentration increases. Despite the change in the reaction products, the amount of *n*-butane dissociation is not enhanced on the carbide-modified Mo(100) surface.[54] A comparison of the reactivity of *n*-butane on Mo(110) and (4×4)-C/Mo(110) has also been carried out.[155] Similar to the Mo(100) surface, the amount of *n*-butane dissociation on both surfaces were found to be ≤0.03 ML.

The discrepancies between the activation of C−H bonds of *n*-butane on carbide-modified V and Mo demonstrate the complex mechanisms of alkane activation over carbide surfaces. One possible explanation for the discrepancies is that they might be related to the differences in the electronic properties of vanadium and molybdenum carbides. For example, the ionic contribution in the metal−nonmetal bonding is greater for vanadium carbide than for molybdenum carbide (section 4.1). NEXAFS results (see Figure 11) also suggest that the degree of broadening of the unfilled states of the metal d band, as a result of carbide formation, is different for the two carbides. Again, detailed investigations of the band structures by IPE, coupled with reactivity studies of alkane molecules, would greatly enhance our understanding of the activation mechanisms of C−H bonds on carbide surfaces.

2. Reactions with Oxygenate Molecules

A detailed understanding of reactions of oxygenates on carbide surfaces is extremely important in evaluating whether the carbide materials can be used as catalysts for partial oxidation of hydrocarbons. Temperature-programmed reaction spectroscopy has been applied to investigate the decomposition mechanisms of formic acid,[65] methanol,[66] formaldehyde,[67] and methyl formate[157] on W(100) and (5×1)-C/W(100). At room temperature, these oxygenate molecules decompose on the clean W(100) surface. The formation of carbide passivates the reactivities of W(100) toward the oxygenate molecules, although substantial decomposition still occurs on the carbide-modified surface. In general, methanol, formaldehyde, and methyl formate were bonded on the (5×1)-C/Mo(100) surface in a similar fashion, most likely through the lone-pair electrons on the oxygen atoms.[67] The decomposition mechanisms of these oxygenate molecules on carbide are different from those on clean W(100), which are often characterized by complicated decomposition mechanisms on the carbide surface.[65−67,157]

For example, Table 4 summarizes the different reaction mechanisms of formaldehyde on W(100) and (5×1)-C/W(100).[67] At low coverages and at 300 K, formaldehyde undergoes complete decomposition on clean W(100) to produce atomic hydrogen, carbon, and oxygen. These atomic species recombine at higher temperatures to desorb as H_2 and CO. On the other hand, formaldehyde adsorbs molecularly on the carbide surface at 300 K. The associatively adsorbed formaldehyde reacts with hydrogen to form methoxy intermediates, which then react to produce methane and methanol. The reaction mechanisms on (5×1)-

Table 4. Reaction Mechanisms of H_2CO on W(100) and (5×1)-C/W(100) at Low Coverages (Reprinted from ref 67. Copyright 1980 Academic.)

temperature regime (K)		
W(100)	W(100)−(5×1)C	reaction
300	NA[a]	$H_2CO(g) \rightarrow 2H(a) + C(a) + O(a)$
300−600	350−600	$2H(a) \rightarrow H_2(g)$
1000	NA	$C(a) + O(a) \rightarrow CO(g)$
	300	$H_2CO(g) \rightarrow H_2CO(a)$
	300	$2H_2CO(a) \rightarrow HCOOCH_3(a)$
	350	$H_2CO(a) \rightarrow 2H(a) + CO(a)$
	350	$H_2CO(a) + H(a) \rightarrow H_3CO(a)$
	350	$H_3CO(a) + H(a) \rightarrow$ complex A, $\rightarrow$ complex B
	350	$H_2CO(a) \rightarrow H_2CO(g)$
	350	$HCOOCH_3(a) \rightarrow HCOOCH_3(g)$
	410	complex A $\rightarrow CH_4(g) + CH_3OH(g) + H_2(g) + O(a) + H_2CO(g)$
	500	complex B $\rightarrow CH_4(g) + CH_3OH(g) + H_2(g) + O(a) + H_2CO(g)$
	410−500	$H_2CO(a) + O(a) \rightarrow HCOO(a) + H(a)$
	545	$HCOO(a) \rightarrow H(a) + CO_2(g)$

[a] Not available.

C/W(100) is further complicated because the adsorbed formaldehyde molecules can also react among themselves to produce methyl formate or react with surface oxygen to produce surface formate. It is also important to point out that the amount of formaldehyde decomposition on the (5×1)-C/W(100) surface is only slightly less than that on clean W(100), which was estimated to be 5.3×10^{14} and 6.1×10^{14} molecules/cm^2, respectively.[67] Overall, the general trends in the reactions of oxygenate molecules are (1) the carbide surfaces are still relatively reactive to the decomposition of oxygenate molecules and (2) the formation of carbide favors hydrocarbon molecules as reaction products.[65−67,157]

3. Reactions with Sulfur- and Nitrogen-Containing Organic Molecules

A fundamental understanding of the reactions of carbide/nitride overlayers with sulfur- and nitrogen-containing organic molecules is of practical importance since it provides information on the hydrodesulfurization (HDS) and hydrodenitrogenation (HDN) activities of these catalysts. For example, it was found that the HDS of thiophene to C4 hydrocarbons (1,3-butadiene, 1-butene, and *n*-butane) and H_2S can be catalyzed by Mo_2C powder catalysts.[158] Kelly et al. have carried out a detailed TPD study of the reaction of thiophene and its HDS products on the carbide-modified Mo(100) surface.[54] Figure 24 shows the thermal desorption of thiophene and H_2 after reactions of submonolayer coverages of thiophene with clean and carbide-modified Mo(100) surfaces. As the carbon coverage increases, the overall peak area for H_2 desorption decreases, which is accompanied by an increase in the peak area of molecular thiophene desorption. These observations indicate that thiophene molecules react more strongly on clean Mo(110) than on carbide-modified Mo(110), although a significant amount of decomposition still occurs even on a carbide surface with a carbon coverage of 0.84 ML. One of the important observations in Figure 24 is that the peak area of the H_2 desorption peak at 690 K shows an increase on the carbide-

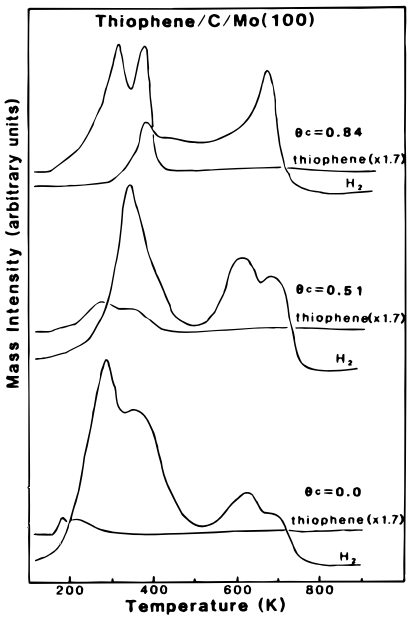

Figure 24. Thermal desorption of molecular thiophene and hydrogen from clean and carbide-modified Mo(100). (Reprinted from ref 54. Copyright 1986 Elsevier.)

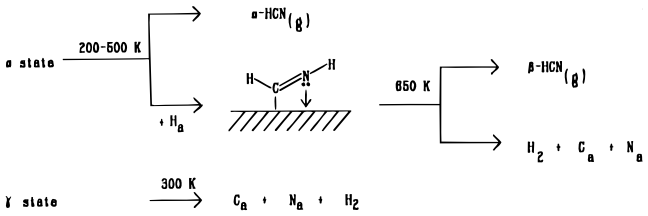

Figure 25. Reaction schemes of HCN on a (5×1)-CW(100) surface. (Reprinted from ref 73. Copyright 1988 American Chemical Society.)

modified surfaces. This high-temperature peak was suggested to be related to the further decomposition of C4 intermediates that were produced from the HDS of thiophene.[54] Further studies using vibrational or photoemission spectroscopies should provide more detailed information on the activation mechanism of C−S bonds on carbide overlayers.

The reactions of nitrogen-containing organic molecules, such as nitriles and amines[69,73,159] have been investigated on carbide-modified W(100) and on nitride-modified Mo(100).[116] Although these studies were not intended to model HDN reactions, they provided information on the activation mechanisms of the C−N bonds on these surfaces. For example, the decomposition mechanisms of nitriles and amines were found to be different for the clean W(100) and (5×1)-C surfaces. Figure 25 shows a comparison of reaction schemes of HCN on the two surfaces. At low coverages on W(100), HCN molecules adsorb in the so-called γ-state, leading to the complete decomposition at 300 K to atomic hydrogen, nitrogen and carbon. The first two atomic species recombine to desorb as H_2 from 300−700 K and as N_2 from 900−1400 K, leaving residual carbon on the surface.[68] On the (5×1)-C/W(100) surface, the stability of molecularly adsorbed HCN and the subsequent decomposition mechanisms are significantly different, particularly at low coverages. As shown in Figure 25, some of the molecularly adsorbed HCN reacts with surface hydrogen to produce a new surface intermediate,

H−C═N−H,[73] which further decomposes at higher temperatures.

Although the above two examples demonstrate that the C−S and C−N bonds can be dissociated on the carbide-modified surfaces, more detailed investigations are needed for an overall understanding of the HDS and HDN mechanisms on these surfaces. Because the HDS/HDN reactions involve the cleavage of C−S/C−N bonds without the dissociation of neighboring carbon−carbon bonds, probing molecules with higher molecular weights (≥5 carbon atoms) should be used in these studies. The HDS and HDN activities of carbides/nitrides, combined with their high sulfur and nitrogen tolerance, might eventually lead to their replacement of noble metals as commercial catalysts.

4. General Similarities and Differences

In general, reactivities of carbide-modified surfaces are significantly different from those of their parent metals. For example, clean surfaces of V, Mo, and W react very strongly with unsaturated hydrocarbons, oxygenates, and organic thiol and nitrile molecules, as shown by the complete decomposition of these molecules at submonolayer coverages. The strong reactivities of the clean surfaces are passivated on carbide-modified surfaces, although the degree of passivation depends on the specific metal substrate and adsorbate. Another common observation is that reactions on carbide-modified surfaces often produce surface intermediates and desorption products that are different from those on the parent metal surfaces. The modified reaction pathways on the carbide surfaces compare more favorably to those of group VIII metals than to their parent metals, especially for the decomposition of unsaturated hydrocarbon molecules.

Despite these general similarities, the reactivities of carbide-modified surface are not identical on all substrate, particularly for the activation of the C−H bonds of alkanes. This might be attributed to the differences in the electronic and structural properties of these carbides. For example, the electronic properties of vanadium carbide are different from those of molybdenum carbide (and most likely tungsten carbide) since the former is characterized by a much more significant ionic contribution in the metal−carbon bonds (Figure 10). Differences in the structures and morphologies of carbide overlayers should also affect the reactivities, such as the different reactivities of the (100) and (111) surfaces of TiC and NbC bulk materials.[33−35,160] A more detailed understanding of the structural information, especially the locations of carbon atoms and the local carbon/metal stoichiometries should provide insightful information on the differences in the reactivities. Finally, the differences in the reactivities of carbide- and nitride-modified Mo(110) surfaces demonstrate that the presence of carbon and nitrogen atoms in the subsurface/interstitial sites is critical for the modeling of the reactivities of bulk carbide and nitride materials.

VI. Future Research Opportunities

As summarized above, despite the very interesting and sometimes unique surface reactivities of the carbide/nitride overlayers, several issues still need to be investigated. Especially, detailed experimental and theoretical band structure investigations, coupled with reactivity studies, would definitely provide important information on the underlying electronic properties that are controlling the reactivities of carbides and nitrides. Furthermore, detailed structural characterization, by using for example the TLEED or STM techniques, is also very critical in achieving an overall understanding of the intimate relationship among the structural, electronic and catalytic properties of carbide and nitride materials.

To correctly model the reactivities of bulk carbides and nitrides, the carbide/nitride overlayers should have nonmetal atoms occupying both surface and subsurface/interstitial sites. Although this can be achieved for the carbide overlayers by annealing to higher temperatures, similar preparation procedures might fail for nitride overlayers due to the facile recombination to desorb as molecular nitrogen, as demonstrated for the N/Mo(110) surface. Nitride overlayers with interstitial nitrogen atoms, such as nitrogen-modified Ti(0001) and W(111) overlayers, should provide a better model system for the reactivity studies. Investigations of the reactivities of these bulk-like nitride overlayers with simple probing molecules such CO and ethylene would enhance the fundamental understanding of the similarities and/or differences between transition metal carbides and nitrides.

Another carbide/nitride system that is of catalytic interest is carbide/nitride overlayers on Fe surfaces. Bulk materials of Fe carbides and nitrides are not as well characterized and do not appear to have similar general electronic and structural properties as those of groups IVB−VIB materials. However, the possible roles of Fe carbides in Fischer−Tropsch synthesis reactions[161] and of Fe nitrides in ammonia synthesis reactions[162] make the Fe carbide/nitride overlayers important model systems for surface science studies. Although the reactions of hydrocarbon molecules[163,164] and ammonia[162] on clean Fe, and on Fe modified with *surface* carbon and nitrogen atoms, have been extensively investigated, research opportunities still exist for a systematic understanding of the relationship between the electronic and catalytic properties of *interstitial* carbide[165] and nitride[166] overlayers on Fe surfaces. Comparisons of these carbide/nitride systems with their groups IVB−VIB counterparts would also enhance our overall understanding of the catalytic properties of transition metal carbides and nitrides.

Another aspect of the catalytic application of carbides and nitrides is that these materials are often used in the mixed phase with oxide, which are commonly referred as metal oxycarbides and oxynitrides.[167] Systematic investigations of the electronic modification of carbides and nitrides by oxygen,[168] and its effect on the catalytic activities of these materials, also represent an important research area.

Finally, due to their unique electronic and mechanical properties, groups IVB−VIB carbides and nitrides have extremely important applications in material sciences. For example, TiN films are often used for the coating of electronic devices.[169−171] In

addition, superconducting properties were reported on thin films of some carbides and nitrides.[172−174] Detailed investigations of the electronic properties of thin carbide and nitride overlayers, and of the modification on the electronic properties upon doping by other elements, might provide fruitful research opportunities for the application of carbides and nitrides as advanced materials.

VII. Acknowledgments

I acknowledge many of my former and current coworkers who have been collaborating with me in investigations of the electronic and catalytic properties of transition metal carbides and nitrides: J. E. Baumgartner, B. E. Bent, R. R. Chiannelli, B. D. DeVries, J. Eng, Jr., B. Frühberger, S. Hantzer, R. Kapoor, S. P. Kelty, C. M. Kim, Z.-M. Liu, S. T. Oyama, P. A. Stevens, M. S. Touvelle, M. D. Weisel, and J. M. White.

VIII. References

(1) 1. Toth, L. E. *Transition Metal Carbides and Nitrides*; Academic Press: New York, 1971.
(2) Oyama, S. T.; Haller, G. L. *Catalysis, Specialist Periodical Reports*; Bond, G. C., Webb, G., Eds.; The Chemical Society: London, 1981; Vol. 5, p 333.
(3) Oyama, S. T. *Catal. Today* **1992**, *15*, 179 and references therein.
(4) Oyama, S. T. *The Chemistry of Transition Metal Carbides and Nitrides*; Blackie Academic and Professional: Glasgow, 1996.
(5) Levy, R. L.; Boudart, M. *Science* **1973**, *181*, 547.
(6) Johansson, L. I. *Surf. Sci. Rep.* **1995**, *21*, 177 and references therein.
(7) Gubanov, V. A.; Ianovsky, A. L.; Zhukov, V. P. *Electronic Structure of Refractory Carbides and Nitrides*; Cambridge University Press: Cambridge, 1994.
(8) Leclercq, L. In *Surface Properties and Catalysis by Nonmetals*; Bonnelle, J. P., Delmon, B., Derouane, E., Eds.; Reidel: Dordrecht, 1983; p 433.
(9) Hägg, G. *Z. Phys. Chem.* **1931**, *12*, 33.
(10) Brewer, L. *Science* **1968**, *161*, 115.
(11) Engel, N. Some New Viewpoints on the Metallic Bond. *Ingenioeren* **1939**, *N101*.
(12) Calais, J.-L. *Adv. Phys.* **1977**, *26*, 847.
(13) Neckel, A. *Int. J. Quantum Chem.* **1983**, *23*, 1317.
(14) Schwarz, K. *CRC Crit. Rev. Solid State Mater. Sci.* **1987**, *13*, 11 and references therein.
(15) Neckel, A.; Rastl, P.; Eibler, R.; Weinberger, P.; Schwarz, K. *J. Phys. C (Solid State Phys.)* **1976**, *9*, 579.
(16) Ramqvist, L. *J. Appl. Phys.* **1971**, *42*, 2113.
(17) Ramqvist, L.; Hamrin, K.; Johansson, G.; Fahlman, A.; Noedling, C. *J. Phys. Chem. Solids* **1969**, *30*, 1835.
(18) Johansson, L. I.; Hagström, A. L.; Jacobsson, B. E.; Hagström, S. B. M. *J. Electron Spectrosc. Related Phenom.* **1977**, *10*, 259.
(19) Benesh, G. A. *Chem. Phys. Lett.* **1992**, *191*, 315.
(20) Chen, J. G.; Kim, C. M.; Frühberger, B.; DeVries, B. D.; Touvelle, M. S. *Surf. Sci.* **1994**, *321*, 145.
(21) Siegel, E. *Semicond. Insul.* **1979**, *5*, 47.
(22) Heine, V. *Phys. Rev.* **1967**, *153*, 673.
(23) Jansen, S. A.; Hoffmann, R. *Surf Sci.* **1988**, *197*, 474 and references therein.
(24) Bonnett, L. H.; Cuthill, J. R.; McAlister, A. J.; Erickson, N. E.; Watson, R. E. *Science* **1974**, *184*, 563.
(25) Colton, R. J.; Huang, J. J.; Rabalais, J. W. *Chem. Phys. Lett.* **1975**, *34*, 337.
(26) Houston, J. E.; Laramore, G. E.; Park, R. L. *Science* **1974**, *185*, 258.
(27) Lee, J. S.; Yeom, M. H.; Park, K. Y.; Nam, I.-S.; Chung, J. S.; Kim, Y. G.; Moon, S. H. *J. Catal.* **1991**, *128*, 126.
(28) Lee, J. S.; Locatelli, S.; Oyama, S. T.; Boudart, M. *J. Catal.* **1990**, *125*, 157.
(29) Ribeiro, F. H.; Dalla Betta, R. A.; Boudart, M.; Baumgartner, J.; Iglesia, E. *J. Catal.* **1991**, *130*, 86.
(30) Markel, E. J.; Van Zee, W. J. *J. Catal.* **1990**, *126*, 643.
(31) Abe, H.; Bell, A. T. *Catal. Lett.* **1993**, *18*, 9.
(32) Schlatter, J. C.; Oyama, S. T.; Metcalfe, J. E., III; Lambert, J. M., Jr. *Ind. Eng. Chem. Res.* **1988**, *27*, 1648.
(33) Kojima, I.; Orita, M.; Miyazaki, E.; Otani, S. *Surf. Sci.* **1985**, *160*, 153.
(34) Oshima, C.; Aono, M.; Tanaka, T.; Kawai, S.; Zaima, S.; Shibata, Y. *Surf. Sci.* **1981**, *102*, 312.
(35) Zaima, S.; Shibata, Y.; Adachi, H.; Oshima, C.; Otani, S.; Aono, M.; Ishizawa, Y. *Surf. Sci.* **1985**, *157*, 380.
(36) Leclercq, L.; Imura, K.; Yoshida, S.; Barbee, T.; Boudart, M. In *Preparation of Catalysts II*; Delmon, B., Grange, P., Jacobs, P. A., Poncelet, G., Eds.; Elsevier: Amsterdam, 1979.
(37) Bohm, H. *Electrochim. Acta* **1970**, *15*, 1273.
(38) Ross, P. N., Jr.; Stonehart, P. *J. Catal.* **1975**, *39*, 298.
(39) Ross, P. N., Jr.; Stonehart, P. *J. Catal.* **1977**, *48*, 42.
(40) Mills, G. A.; Steffgen, F. W. *Catal. Rev.* **1973**, *8*, 159.
(41) Palanker, V. S. H.; Gayev, R. A.; Sokolsky, D. V. *Electrochim. Acta* **1977**, *22*, 133.
(42) Ranhotra, G. S.; Haddix, G. W.; Bell, A. T.; Reimer, J. A. *J. Catal.* **1987**, *108*, 24.
(43) Chen, J. G.; Frühberger, B.; Weisel, M. D.; Baumgartner, J. E.; DeVries, B. D. *The Chemistry of Transition Metal Carbides and Nitrides*; Blackie Academic and Professional: Glasgow, 1996; p 439.
(44) Chen, J. G.; Weisel, M. D.; Liu, Z.-M.; White, J. M. *J. Am. Chem. Soc.* **1993**, *115*, 8875.
(45) Chen, J. G. *J. Catal.* **1995**, *154*, 80.
(46) Chen, J. G.; DeVries, B. D.; Frühberger, B.; Kim, C. M.; Liu, Z.-M. *J. Vac. Sci. Technol. A* **1995**, *13*, 1600.
(47) Londry, F. A.; Slavin, A. J.; Underhill, P. R. *Surf. Sci.* **1984**, *140*, 521.
(48) Ko, E. I.; Madix, R. J. *Surf. Sci.* **1980**, *100*, L449.
(49) Ko, E. I.; Madix, R. J. *Surf. Sci.* **1981**, *109*, 221.
(50) Ko, E. I.; Madix, R. J. *Surf. Sci.* **1981**, *112*, 373.
(51) Overbury, S. H.; Stair, P. C. *J. Vac. Sci. Technol.* A **1983**, *1*, 1055.
(52) Grant, J. L.; Fryberger, T. B.; Stair, P. C. *Surf. Sci.* **1985**, *159*, 333.
(53) Guillot, C.; Riwan, R.; Lecante, J. *Surf. Sci.* **1976**, *59*, 581.
(54) Kelly, D. G.; Salmeron, M.; Somorjai, G. A. *Surf. Sci.* **1986**, *175*, 465.
(55) Kellogg, D. S.; Touvelle, M. S.; Stair, P. C. *J. Catal.* **1989**, *120*, 192.
(56) Jentz, D.; Rizzi, S.; Barbieri, A.; Kelly, D. G.; Van Hove, M. A. Somorjai, G. A. *Surf. Sci.* **1995**, *329*, 14.
(57) Young, M. B.; Slavin, A. J. *Surf. Sci.* **1991**, *245*, 56.
(58) He, J.-W.; Kuhn, W. K.; Goodman, D. W. *Surf. Sci.* **1992**, *262*, 351.
(59) Frühberger, B.; Chen, J. G. *Surf. Sci.* **1995**, *342*, 38.
(60) Frühberger, B.; Chen, J. G.; Eng, J., Jr.; Bent, B. E. *J. Vac. Sci. Technol.*, in press.
(61) Overbury, S. H. *Surf. Sci.* **1987**, *184*, 319.
(62) Ollis, D. F.; Boudart, M. *Surf. Sci.* **1970**, *23*, 320.
(63) Bauer, E. *Surf. Sci.* **1967**, *7*, 351.
(64) Benziger, J. B.; Ko, E. I.; Madix, R. J. *J. Catal.* **1978**, *54*, 414.
(65) Benziger, J. B.; Ko, E. I.; Madix, R. J. *J. Catal.* **1979**, *58*, 149.
(66) Ko, E. I.; Benziger, J. B.; Madix, R. J. *J. Catal.* **1980**, *62*, 264.
(67) Benziger, J. B.; Ko, E. I.; Madix, R. J. *J. Catal.* **1980**, *64*, 132.
(68) Baldwin, E. K.; Friend, C. M. *J. Phys. Chem.* **1987**, *91*, 3821.
(69) Pearlstine, K. A.; Friend, C. M. *J. Phys. Chem.* **1986**, *90*, 4341; **1986**, *90*, 4344.
(70) Pearlstine, K. A.; Friend, C. M. *J. Am. Chem. Soc.* **1985**, *107*, 5898.
(71) Friend, C. M.; Serafin, J. G.; Baldwin, E. K.; Stevens, P. A.; Madix, R. J. *J. Chem. Phys.* **1987**, *87*, 1847.
(72) Pearlstine, K. A.; Friend, C. M. *J. Vac. Sci. Technol.* A. **1984**, *2*, 1021.
(73) Serafin, J. G.; Friend, C. M. *J. Phys. Chem.* **1988**, *92*, 6694.
(74) Chesters, M. A.; Hopkins, B. J.; Taylor, P. A.; Winton, R. I. *Surf. Sci.* **1979**, *83*, 181.
(75) Mullins, D. R.; Overbury, S. H. *Surf. Sci.* **1988**, *193*, 455.
(76) Stefan, P. M.; Spicer, W. E. *Surf. Sci.* **1985**, *149*, 423.
(77) Baudoing, R.; Stern, R. M. *Surf. Sci.* **1968**, *10*, 392.
(78) MacMillan, J. G.; Slavin, A. J.; Sunderland, K. J. *Surf. Sci.* **1986**, *173*, 138.
(79) Sunderland, K. J.; Slavin, A. J. *Surf. Sci.* **1990**, *233*, 233.
(80) Foulias, S. D.; Rawlings, K. J.; Hopkins, B. J. *Surf. Sci.* **1983**, *133*, 377.
(81) Backyx, C.; Willis, R. F.; Feuerbacher, B. F.; Fitton, B. *Surf. Sci.* **1977**, *68*, 516.
(82) Haas, T. W.; Grant, J. T. *Appl. Phys. Lett.* **1970**, *16*, 172.
(83) Grant, J. T.; Haas, T. W. *Surf. Sci.* **1971**, *24*, 332.
(84) Stohr, J. *NEXAFS Spectroscopy*; Springer Series in Surface Science 25; Springer Verlag: New York, 1992.
(85) Rosenberg, R. A.; Love, P. J.; Rehn, V. *Phys. Rev. B* **1986**, *33*, 4034.
(86) Willis, R. F.; Fitton, B.; Painter, G. S. *Phys. Rev. B* **1974**, *9*, 1926.
(87) Fink, J.; Muller-Heinzerling, T.; Pfluger, J.; Bebenzer, A.; Koidl, P.; Grecelius, G. *Solid State Commun.* **1983**, *9*, 687.
(88) Comelli, G.; Stohr, J.; Robinson, C. J.; Jark, W. *Phys. Rev. B.* **1988**, *38*, 7511.
(89) Kapoor, R.; Oyama, S. T.; Frühberger, B.; DeVries, B. D.; Chen, J. G. *Catal. Lett.* **1995**, *34*, 179.
(90) Pflüger, J.; Fink, J.; Crecelius, G.; Bohnen, K. P.;Winter, H. *Solid State Commun.* **1982**, *44*, 489.
(91) Pflüger, J.; Fink, J.; Schwarz, K. *Solid State Commun.* **1985**, *55*, 675.

(92) Fischer, D. A.; Colbert, J.; Gland, J. L. *Rev. Sci. Instrum*. **1989**, *60*, 1596.
(93) Ertl, G.; Küppers, J. *Low Energy Electrons and Surface Chemistry*; Monographs in Modern Chemistry 4; Verlag Chemie: New York, 1974, p7.
(94) Veigele, W. J. *At. Data Nucl. Data Tables*, **1973**, *5*, 51.
(95) Fukuda, Y.; Honda, F.; Rabalais, J. W. *Surf. Sci*. **1980**, *91*, 165.
(96) Foord, J. S.; Goddard, P. J.; Lambert, R. M. *Surf. Sci*. **1980**, *94*, 339.
(97) King, D. A.; Tompkins, F. C. *Trans. Faraday Soc*. **1968**, *64*, 496
(98) Eastman, D. E. *Solid State Commun*. **1972**, *10*, 933.
(99) Brealey, W.; Surplice, N. A. *Surf. Sci*. **1977**, *64*, 372.
(100) Fudaka, Y.; Elam, W. T.; Park, R. L. *Appl. Surf. Sci*. **1978**, *1*, 278.
(101) Shih, H. D.; Jona, F.; Jepsen, D. W.; Marcus, P. M. *Phys. Rev. Lett*. **1976**, *36*, 798.
(102) Shih, H. D.; Jona, F.; Jepsen, D. W.; Marcus, P. M. *Surf. Sci*. **1976**, *60*, 445.
(103) Shih, H. D.; Legg, K. O.; Jona, F. *Surf. Sci*. **1976**, *54*, 355.
(104) Rao, G. R.; Rao, C. N. R. *J. Phys. Chem*. **1990**, *94*, 7986.
(105) Fromm, E.; Mayer, O. *Surf. Sci*. **1978**, *74*, 259.
(106) Posternak, R. A.; Gibson, R. *Acta Metall*. **1965**, *13*, 1031.
(107) Farell, H. H.; Isaacs, H. S.; Strogin, M. *Surf. Sci*. **1973**, *38*, 31.
(108) Dickey, J. M. *Surf. Sci*. **1975**, *50*, 515.
(109) Ko, S. M.; Schmidt, L. D. *Surf. Sci*. **1974**, *42*, 508.
(110) Ko, S. M.; Schmidt, L. D. *Surf. Sci*. **1975**, *47*, 557.
(111) Alessandrini, E. I.; Brusic, V. *J. Vac. Sci. Technol*. **1971**, *9*, 83.
(112) Gewinner, G.; Peruchetti, J. C.; Riedinger, R.; Jaegle, A. *Solid State Commun*. **1980**, *36*, 785.
(113) Fukuda, Y.; Nagoshi, M. *Surf. Sci*. **1988**, *203*, L651.
(114) Miyano, T.; Kamei, K.; Sakisaka, Y.; Onchi, M. *Surf. Sci*. **1984**, *148*, L645.
(115) Shinn, N. D. *Phys. Rev. B* **1990**, *41*, 9771.
(116) Bafrali, R.; Bell, A. T. *Surf. Sci*. **1992**, *278*, 353; **1994**, *316*, 267.
(117) Abon, M.; Bergeret, G.; Tardy, B. *Surf. Sci*. **1977**, *68*, 305.
(118) Frühberger, B.; Colaianni, M. L.; Chen, J. G. *Phys. Rev. B*., to be submitted.
(119) Egawa, C.; Naito, S.; Tamaru, K. *Surf. Sci*. **1983**, *125*, 605.
(120) McAllister, J.; Hansen, R. S. *J. Chem. Phys*. **1973**, *59*, 414.
(121) Grunze, M.; Brundle, C. R.; Tomanek, D. *Surf. Sci*. **1982**, *119*, 133.
(122) Pfnür, H. E.; Rettner, C. T.; Lee, J.; Madix, R. J.; Auerbach, D. J. *J. Chem. Phys*. **1986**, *85*, 7452.
(123) Somerton, C.; King, D. A. *Surf. Sci*. **1979**, *89*, 391.
(124) Lee, J.; Madix, R. J.; Schlaegel, J. E.; Auerbach, D. J. *Surf. Sci*. **1984**, *143*, 626.
(125) Tamm, P. W.; Schmidt, L. D. *Surf. Sci*. **1971**, *26*, 286.
(126) Cosser, R. C.; Bare, S. R.; Francis, S. M.; King, D. A. *Vacuum* **1981**, *31*, 503.
(127) Boudart, M.; Egawa, C.; Oyama, S. T.; Tamaru, K. *J. Chim. Phys*. **1981**, *78*, 987.
(128) Choi, J.-G.; Lee, H. J.; Thompson, L. T. *Appl. Surf. Sci*. **1994**, *78*, 299.
(129) Donovan, E. P.; Hubler, G. K.; Mudholkar, M. S.; Thompson, L. T. *Surf. Coat. Technol*. **1994**, *66*, 499.
(130) Lee, H. J.; Choi, J.-G.; Colling,C. W.; Mudholkar, M. S.; Thompson, L. T. *Appl. Surf. Sci*. **1995**, *89*, 121.
(131) Hitchcock, A. P.; Brion, C. E. *J. Electron Spectrosc. Relat. Phenom*. **1980**, *18*, 1.
(132) Wight, C. R.;Brion, C. E. *J. Electron Spectrosc. Relat. Phenom*. **1974**, *4*, 25.
(133) Sariano, L.; Abbate, M.; Fuggle, J. C.; Jimenez, C.; Sanz, J. M.; Galan, L.; Mythen, C.; Padmore, H. A. *Surf. Sci*. **1993**, *281*, 120.
(134) Sanderson, R. T. *J. Am. Chem. Soc*. **1952**, *74*, 272.
(135) Parr, R. G.; Donnelly, R. A.; Levy, M.; Palke, W. E. *J. Chem. Phys*. **1978**, *68*, 3801.
(136) Chen, J. G. *Surf. Sci. Reports*, in preparation.
(137) Nyberg, C. *Surf. Sci*. **1979**, *82*, 165.
(138) Capuzano, J. C. in *The Chemical Physics of Solid Surf.s and Interfaces and Heterogeous Catalysis*; King, D. A.. Woodruff, D. P., Eds.; Elsevier: Amsterdam, 1990; Vol. 3A, p 389.
(139) Sheppard, N.; Nruyen, T. T. In *Adv. Infrared Raman Spectrosc.* **1979**, *5*, 67.
(140) Broden, G.; Phodin, T. N.; Brucker, C.; Benbow, R.; Hurych, Z. *Surf. Sci*. **1976**, *59*, 593.
(141) Sung, S.; Hoffmann, R. *J. Am. Chem. Soc*. **1985**, *107*, 578.
(142) Herzberg, G. *Molecular Spectra and Molecular Structure*; 2nd ed.; Van Nostrand Reinhold Company Inc.: New York, 1950; Vol. 1.
(143) Chen, J. G.; Colaianni, M. L.; Weinberg,W. H.; Yates, Jr., J. T. *Chem. Phys. Lett*. **1991**, 177, 113.
(144) Colaianni, M. L.; Chen, J. G.; Weinberg,W. H.; Yates, J. T., Jr. *J. Am. Chem. Soc*. **1992**, *114*, 3735.
(145) Jones, L. H.; McDowell, R. S.; Goldblatt, M. *Inorg. Chem*. **1969**, *8*, 2340.
(146) Sheppard, N. *Annu. Rev. Phys. Chem*. **1988**, *39*, 589 and references therein.
(147) Frühberger, B.; Chen, J. G. *J. Am. Chem. Soc*. submitted for publication.
(148) Blomberg, M. R. A.; Siegbahn, P. E. M.; Svenssson, M. *J. Phys. Chem*. **1992**, *96*, 9794.
(149) Steininger, H.; Ibach, H.; Lehwald, S. *Surf. Sci*. **1982**, *117*, 685.
(150) Skinner, P.; Howard, M. W.; Oxton, I. A.; Kettle, S. F. A.; Powell, D. B.; Sheppard, N. *J. Chem. Soc. Faraday Trans. 2* **1981**, *77*, 397.
(151) Eng, J., Jr.; Bent, B. E.; Frühberger, B.; Chen, J. G. Manuscript in preparation.
(152) Xu, C.; Koel, B. E. *Surf. Sci*. **1994**, *304*, 249 and references therein.
(153) Eng, J., Jr.; Bent, B. E.; Frühberger, B.; Chen, J. G. *J. Phys. Chem*., submitted for publication.
(154) Tsai, M.-C.; Stein, J.; Friend, C. M.; Muetterties, E. L. *J. Am. Chem. Soc*. **1982**, *104*, 3533.
(155) Chen, J. G.; Frühberger, B.; Eng, J., Jr.; Bent, B. E. Manuscript in preparation.
(156) Brookhart, M.; Green, M. L. H.; Wong, L.-L. *Prog. Inorg. Chem*. **1988**, *36*, 1.
(157) Barteau, M.; Madix, R. J. *J. Catal*. **1980**, *62*, 329.
(158) Lee, J. S.; Boudart, M. *Appl. Catal*. **1983**, *19*, 207.
(159) Friend, C. M.; Serafin, J. G. *J. Chem. Phys*. **1988**, *88*, 4037.
(160) Oshima, C.; Aono, M.; Zaima, S.; Shibata, Y.; Kawai, S. *J. Less-Common Met*. **1981**, *82*, 69.
(161) See, for example: Dry, M. E. in *Catalysis, Science and Technology*; Anderson, J. R., Boudart, M., Eds.; Springer: Berlin, 1981; Vol. 1.
(162) See, for example: Weiss, M.; Ertl, G.; Nitschke, F. *Appl. Surf. Sci*. **1979**, *2*, 614.
(163) Seip, U.; Tsai, M.-C.; Küppers, J.; Ertl, G. *Surf. Sci*. **1984**, *147*, 65.
(164) Kuivila, C. S.; Butt, J. B.; Stair, P. C. *Appl Surf. Sci*. **1988**, *32*, 99.
(165) Geib, K. M.; Wilmsen, C. W. *Surf. Sci. Spectra* **1992**, *1*, 297.
(166) Diekmann, W.; Panzner, G.; Grabke, H. J. *Surf. Sci*. **1989**, *218*, 507.
(167) Iglesia, E.; Rebeiro, F. H.; Boudart, M.; Baumgartner, J. E. *Catal. Today*, **1992**, *15*, 307.
(168) See, for example: Souda, R.; Aizawa, T.; Otani, S.; Ishizawa, Y. *Surf. Sci*. **1991**, *256*, 19.
(169) Truong, C. M.; Chen, P. J.; Corneille, J. S.; Oh, W. S.; Goodman, D. W. *J. Phys. Chem*. **1995**, *99*, 8831.
(170) Jouan, P.-Y.; Peignon, M.-C.; Cardinaud, Ch.; Lemperiere, G. *Appl. Surf. Sci*. **1993**, *68*, 595.
(171) Strydom, I. I. R.; Hofmann, S. *Vacuum* **1990**, *41*, 1619.
(172) Saito, K.; Yabe, K.; Nishimura, O. *Nucl. Instrum. Methods Phys. Res. B* **1989**, *39*, 623.
(173) Allison, C. Y.; Finch, C. B.; Foegelle, M. D.; Modine, F. A. *Solid State Commun*. **1988**, *68*, 387.
(174) Garwin, E. L.; King, F. K.; Kerby, R. E.; Aita, O. *J. Appl. Phys*. **1987**, *61*, 1145.

CR950232U